Quantitative Assessment of Coronary Microvascular Function

Dynamic Single-Photon Emission Computed Tomography, Positron Emission Tomography, Ultrasound, Computed Tomography, and Magnetic Resonance Imaging

Attila Feher, MD, PhD; Albert J. Sinusas, MD

***Abstract*—**A healthy, functional microcirculation in combination with nonobstructed epicardial coronary arteries is the prerequisite of normal myocardial perfusion. Quantitative assessment in myocardial perfusion and determination of absolute myocardial blood flow can be achieved noninvasively using dynamic imaging with multiple imaging modalities. Extensive evidence supports the clinical value of noninvasively assessing indices of coronary flow for diagnosing coronary microvascular dysfunction; in certain diseases, the degree of coronary microvascular impairment carries important prognostic relevance. Although, currently positron emission tomography is the most commonly used tool for the quantification of myocardial blood flow, other modalities, including single-photon emission computed tomography, computed tomography, magnetic resonance imaging, and myocardial contrast echocardiography, have emerged as techniques with great promise for determination of coronary microvascular dysfunction. The following review will describe basic concepts of coronary and microvascular physiology, review available modalities for dynamic imaging for quantitative assessment of coronary perfusion and myocardial blood flow, and discuss their application in distinct forms of coronary microvascular dysfunction. **(*Circ Cardiovasc Imaging*. 2017;10:e006427. DOI: 10.1161/CIRCIMAGING.117.006427.)**

Key Words: coronary flow reserve ■ coronary microvascular function ■ microvascular dysfunction ■ myocardial blood flow ■ myocardial perfusion imaging

Coronary Microvascular Physiology and Microvascular Disease

Myocardial perfusion is tightly regulated by dynamic and integrated changes in the epicardial and intramyocardial coronary vasculature and downstream microcirculation. During resting conditions, roughly 75% of the oxygen is extracted from the blood by the myocardium, which leaves minimal reserve for additional oxygen extraction. Therefore, any increase in oxygen consumption/cardiac metabolism leading to increased oxygen demand can only be matched by increase in myocardial blood flow (MBF). The regulation of MBF largely resides in the microcirculation. As illustrated by Figure 1, epicardial coronaries (500 μm to 5 mm) represent negligible part (≈10%) of the coronary resistance to flow when no obstructive stenosis is present. The capillary system and venules offer minimal resistance as well, serving as capacitance vessels by holding 90% of the total intramyocardial blood volume (IMBV). Consequently, under normal conditions, the coronary vascular resistance is primarily controlled by prearterioles (diameter 100–500 μm) and arterioles (<100 μm). In the presence of stable determinants of myocardial oxygen consumption, MBF remains relatively constant over a wide range of coronary perfusion pressures as a result of autoregulation (Figure 2). Autoregulation is achieved by dynamic regulation of the coronary microvascular diameter at the prearteriolar level through shear stress (flow-mediated dilation) and pressure-dependent (myogenic response) intrinsic mechanisms. Below the lower pressure limit of autoregulation, coronary flow decreases exponentially, resulting in myocardial ischemia. Therefore, there is a complex control of the resistance in the coronary arterial tree and microcirculation that involves shear-mediated neurohormonal regulation, metabolic regulation, and myogenic control.

In the presence of epicardial disease or microvascular disease, the coronary flow reserve (CFR) is determined by the maximum hyperemic blood flow divided by the baseline coronary flow (Figure 2). The normal value of CFR greatly depends on the technique used for quantification, but most publications consider CFR<2.0 sufficiently abnormal to result in ischemia.[1] As depicted in Figure 2, baseline flow conditions

Received March 13, 2017; accepted June 26, 2017.

From the Section of Cardiovascular Medicine, Department of Internal Medicine (A.F., A.J.S.) and Department of Radiology and Biomedical Imaging (A.J.S.), Yale University School of Medicine, New Haven, CT.

Correspondence to Albert J. Sinusas, MD, Section of Cardiovascular Medicine, Yale University School of Medicine, PO Box 208017, Dana 3, New Haven, CT 06520. E-mail albert.sinusas@yale.edu

Circ Cardiovasc Imaging **is available at http://circimaging.ahajournals.org** **DOI: 10.1161/CIRCIMAGING.117.006427**

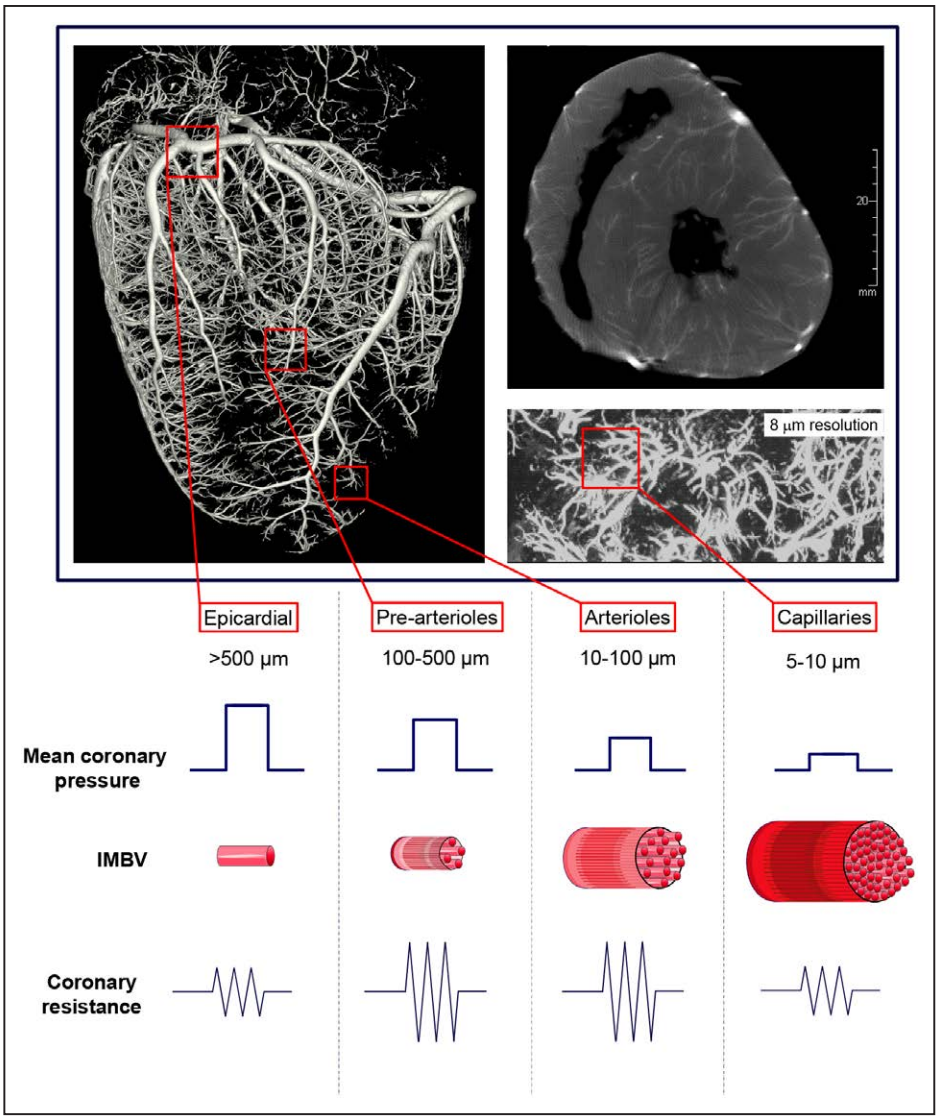

Figure 1. Functional components of the coronary arterial system. Three-dimensional (3D) volume rendering of contrast microCT of porcine heart (**top left**), with maximum intensity projection of axial slice (**top right**), and ultrahigh resolution microCT images (**bottom right**). The porcine heart was perfused with 5% bismuth containing casting medium. The functional components of the coronary vascular tree are defined based on segregation of vascular tree by vascular diameter. Under physiological conditions, the majority of intramyocardial blood volume (IMBV) resides in arterioles and capillaries, whereas the most important contributors to coronary resistance are prearterioles and arterioles. Epicardial coronaries contribute to resistance and IMBV minimally. CT indicates computed tomography.

have significant impact on CFR; any rise in baseline MBF can lead to underestimation of true CFR.

The other cornerstone of reliably estimating CFR is the achievement of maximum hyperemia. If full hyperemia is not present during vasodilator or exercise stress, CFR and the functional severity of epicardial stenosis may be underestimated. The most frequently used stress agents achieve maximum hyperemia via endothelium-independent vasodilation (adenosine, regadenoson, and dipyridamole).[2] Adenosine has a short half-life (measured in seconds) and is administered as a constant infusion, producing a relatively stable hyperemic state. Adenosine initiates vasodilation via binding to A2 adenosine receptors on coronary smooth muscle cells. However, adenosine can induce unwanted side effects by extracardiac activation of other adenosine receptor subtypes, including activation of A1 receptors causing heart block and A2b receptors causing peripheral vasodilation and bronchiolar constriction. Fortunately, because of the short half-life of adenosine, discontinuation of the adenosine infusion results in a rapid clearance from the circulation and rapid dissipation of adverse off-target effects. Regadenoson is a selective A2a receptor agonist, which is now frequently used for vasodilator stress in conjunction with myocardial perfusion imaging (MPI) and demonstrates less unwanted side effects. However, regadenoson has a longer half-life, is generally administered as a slow bolus, and produces a more variable vasodilator response.[3] The application of regadenoson for determination of absolute flow is more limited, with a recent study suggesting potentially suboptimal hyperemic effect compared with dipyridamole.[4] Dipyridamole inhibits cellular uptake of adenosine, thereby, facilitating intrinsic adenosine-induced vasodilation of intramural coronary

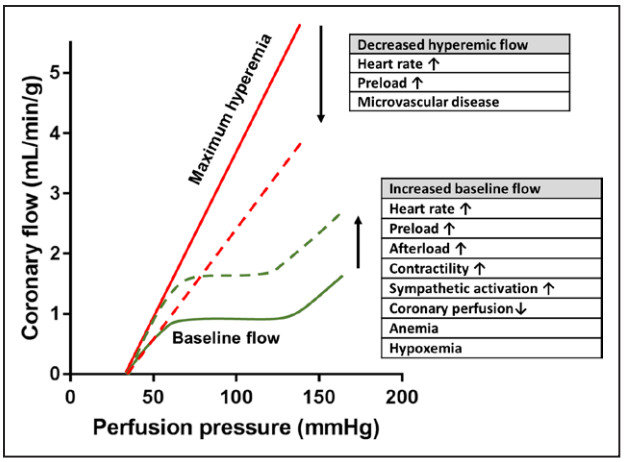

Figure 2. Coronary autoregulation and determinants of coronary flow reserve (CFR). Over the autoregulation range (the plateau of the autoregulation curve), coronary flow remains relatively constant, despite changes in coronary perfusion pressure. CFR is determined by maximum hyperemic blood flow (solid red line) divided by baseline flow (solid green line). Increasing metabolic demand and reduced oxygen/nutrient delivery result in compensatory rise in baseline coronary flow (dashed green line). Increased baseline flow leads to a reduced CFR presuming stable or reduced hyperemic flow. Reduction in hyperemic coronary flow (dashed red line) can be induced by reduced diastolic filling time or coronary microvascular disease and will also result in a decreased CFR.

arterioles inducing near-maximal hyperemia for a more extended period of time. It has to be noted that the level of maximum coronary blood flow is in linear relationship with coronary perfusion pressure; therefore, any peripheral vasodilation leading to hypotension can theoretically underestimate CFR. Unlike the previously mentioned vasodilators, dobutamine raises coronary flow by increasing cardiac workload via β-adrenergic receptor activation, mimicking exercise-induced physiological changes.[2] However, both exercise and dobutamine have been reported to underperform in terms of coronary flow augmentation when compared with adenosine or dipyridamole.

A less frequently used parameter for the description of epicardial stenosis is relative CFR, which is calculated by dividing the maximum stress flow in a diseased artery segment by the maximum coronary flow without the presence of the disease (either in the nondiseased segment of the reference artery or in adjacent artery distribution).[5] Without diffuse atherosclerotic disease, for a discrete stenosis, the relative CFR should be identical to the pressure-derived fractional flow reserve (FFR).[5] Therefore, relative CFR is particularly useful for the characterization of a distinct stenosis, whereas absolute CFR is more informative for the description of coronary pathologies with global involvement, such as coronary microvascular dysfunction (CMVD).

Endothelial function assessment can be performed by combining noninvasive flow quantification methods with cold pressor testing (CPT).[2] This involves immersing the patient's hand or foot in ice cold water, which leads to elevation of blood pressure and heart rate. This induces flow-mediated prearteriolar coronary vasodilation, which can be detected by dynamic imaging. Impaired CPT response has been demonstrated in multiple disease states associated with coronary microvascular pathology.[6–10]

IMBV is defined as the fraction of myocardium volume that is occupied by blood. Ex vivo radiolabeled red blood cell studies (usually performed by labeling RBCs with ^{99m}Tc) have been considered as the gold standard for validation of IMBV estimation because the RBCs stay in the intravascular circulation.[11] At equilibrium, IMBV can be estimated by single-photon emission computed tomography (SPECT) as the tracer concentration in the myocardium over the tracer concentration in the blood pool. Myocardial contrast echocardiography (MCE) uses intravascular gas-filled microbubbles to estimate IMBV.[12,13] IMBV can also be estimated noninvasively from first-pass perfusion CMR[14] and by fast volumetric computed tomography (CT) acquisition.[15] There is limited evidence suggesting that absolute quantification of IMBV might be able to provide additional information about microvascular function beyond that provided by standard qualitative MPI. This is based on the observed approximate doubling of resting IMBV in the presence of critical stenosis,[16] while primary CMVD is associated with a decrease in IMBV.[17]

CT imaging can provide additional novel diagnostic markers to help differentiating coronary artery disease (CAD) from CMVD. Transluminal attenuation gradient, defined as the linear regression coefficient between luminal contrast attenuation (measured in Hounsfield units) and axial distance on coronary CT angiography images, is a novel CT marker used for the evaluation of the degree of coronary stenosis.[18] It is particularly useful in the assessment of calcified stenotic lesions. The application of computational fluid dynamics to contrast CT angiography can also provide a unique opportunity for noninvasive estimation of FFR.[19] As transluminal attenuation gradient and CT-FFR are markers of epicardial stenosis, it is reasonable to assume that they are not affected by alterations in the microcirculation.

CMVD is characterized by an impaired microvascular and suboptimal coronary vasodilator response to exercise or pharmacological stress. Historically, the diagnosis of CMVD required invasive coronary angiography linked with thermodilution or Doppler-based coronary flow assessment (invasive CFR). However, with almost 30 years of experience, noninvasive flow quantification (noninvasive CFR, occasionally called myocardial flow or perfusion reserve) with positron emission tomography (PET) became an alternative gold standard for the assessment of CFR. Currently, no general consensus exists about optimal cutoff values that could be used for the definition of CMVD. Determining a unified diagnostic range for normal CFR is problematic because it is affected by multiple factors, including (1) the method used for its determination, (2) age, (3) sex, (4) rate–pressure product, (5) unrecognized cardiovascular risk factors in supposedly healthy individuals, and (6) test–retest variability. Interestingly, the most frequently used cutoff (CFR<2.5) originates from a small study by Bergmann et al,[20] which identified CFR of 4.1±1.2 in 11 healthy volunteers by performing O^{15}-labeled water imaging with PET. This cutoff has been subsequently used in multiple studies for the diagnosis of CMVD in chest pain patients without obstructive CAD.[21,22] A recent review by Gould et al[5] summarizing data from over 250 publications with PET flow quantification

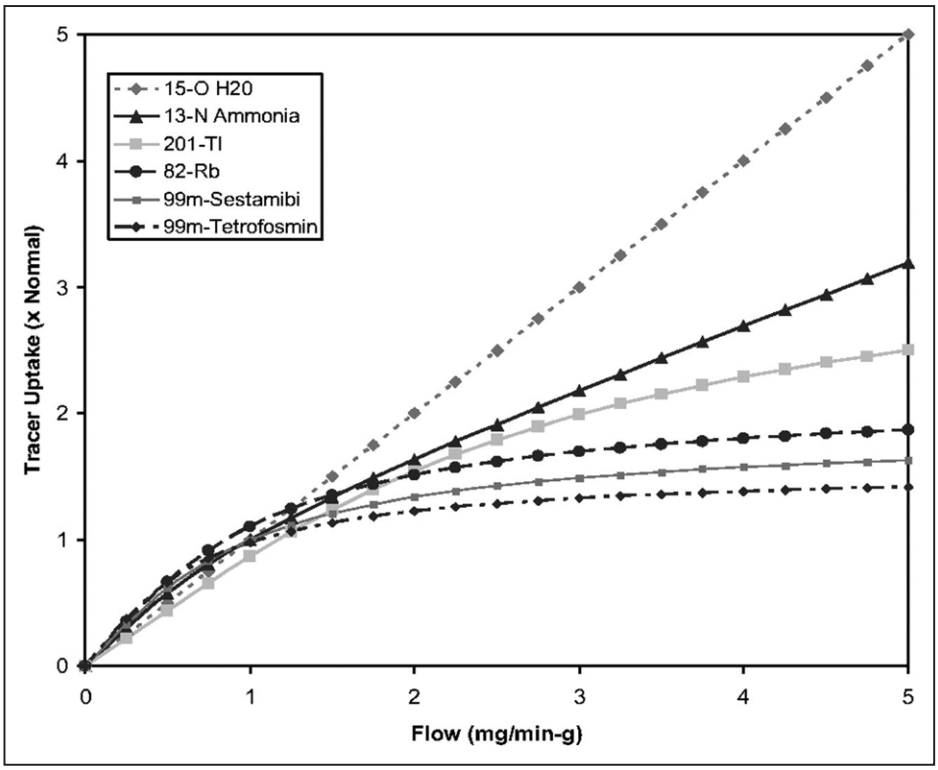

Figure 3. Relationship between myocardial blood flow and tracer uptake for common single-photon emission computed tomography (SPECT) and positron emission tomography (PET) radiotracers demonstrates a roll-off phenomenon at high flow rates because uptake of some radiotracers becomes diffusion limited at higher flows. This results in reduced accuracy in the quantification of hyperemic coronary flow and coronary flow reserve (CFR). Adapted from Salerno et al[2] with permission of the publisher. Copyright ©2009, The American Heart Association, Inc.

demonstrated a CFR of 3.55±1.36 as the weighted average of CFR measurements of nearly 3500 healthy controls. The goal of this review is to discuss the currently available noninvasive methods for the quantification of MBF and to summarize the available noninvasive flow data based on the underlying pathophysiology of CMVD.

Quantification of Flow With Radiotracer Imaging

Ideal Radiotracer and Ideal Acquisition Technique for Dynamic Radiotracer Imaging

Of critical importance, the ideal quantitative MPI agent should have a quantifiable concentration that increases linearly with coronary flow over a large range of flow values. Ideally, the tracer should have a high first-pass extraction without significant recirculation. Of note, for most clinically used radiotracers with increasing coronary flow levels, (1) a competitive back diffusion into blood can be observed after the myocardial tracer uptake or (2) the uptake mechanism of tracer becomes saturated. These mechanisms can result in a progressive decline in myocardial extraction and retention at higher flow rates (roll-off phenomenon; Figure 3).[2] The ideal tracer should show minimal roll-off phenomenon at higher stress-induced flows. The tracer kinetics ideally are not affected by changes in metabolism or type of pharmacological stress, and the agent should demonstrate rapid clearance from the blood pool. The ideal tracer has low extracardiac uptake (especially liver and lung uptake, given their relative proximity to the heart). Last but not the least, the ideal perfusion agent should be safe without significant side effects, stable, and easy to produce at low cost.

The ideal dynamic imaging modality for MBF assessment has high sensitivity to detect small changes in coronary flow. Based on the detected signal, it should be able to quantify perfusion. Ideally, the imaging modality should have high spatial resolution to be able to detect regional and transmural differences in flow, as well as adequate temporal resolution to accurately create time–intensity curves if first-pass imaging is used for flow quantification. The measurement should be reproducible and would need to have high diagnostic utility free of artifacts. It should be widely available, fast, easy to use, cost-effective, and result in low radiation exposure.

Compartmental Modeling of Tracer Kinetics

The dynamic exchange of the tracer between the arterial blood and the myocardium can be described by using compartmental models. Compartmental models give mathematical description about the behavior of the tracer. Based on known or assumed knowledge about tracer kinetics, the body is divided into different compartments that represent either distinct physical space or a metabolic/bound state of the tracer. The amount of tracer leaving any compartment is assumed to be proportional to the concentration in the actual compartment. The constant of this proportionality (the rate constant) describes the fraction

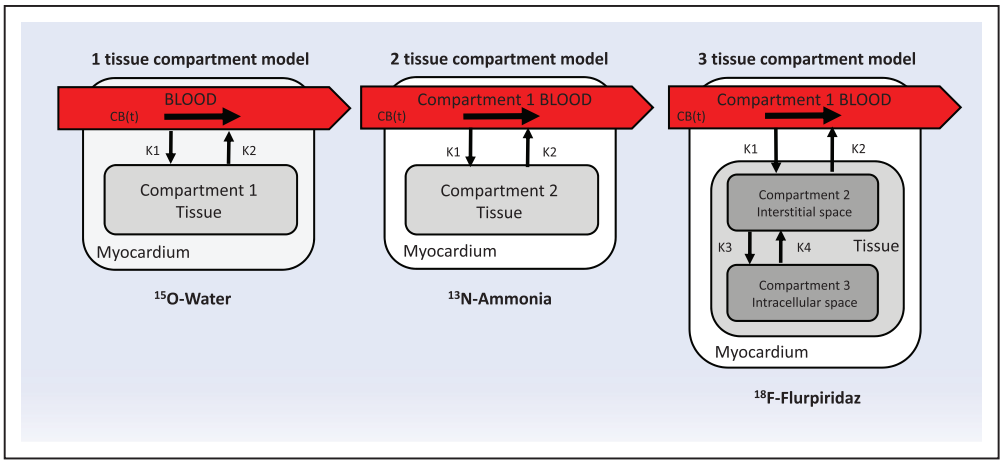

Figure 4. Schematic display of tissue compartment models used in quantitative analysis of dynamic positron emission tomography (PET) imaging of selected PET radiotracers with unique properties. ^{15}O water is a freely diffusible agent, as the blood concentration (CB(t)) is determined by an independent model, the 1 tissue compartment model is used (**left**). ^{13}N ammonia readily diffuses across cell membranes, gets metabolically trapped in the myocardium (compartment 2) with high retention rate (**middle**). After injection and diffusion through capillary membranes, ^{18}F-Flurpiridaz gets trapped intracellularly in the mitochondria by irreversible binding to mitochondrial complex-1 (**right**).

of the tracer that leaves the compartment per unit of time. The uptake constant k1 describes the rate of transfer from blood to tissue, while k2 is the washout rate by blood from tissue. The arterial blood concentration can be measured from direct blood sampling or estimated by fitting input function to the measured activity in the left ventricular (LV) cavity, left atrial cavity, or the aorta. The one compartment model operates with the assumption that the blood concentration is known because the kinetics of the blood concentration is determined by an independent model. Therefore, the only unknown variable is the tissue concentration (Figure 4). The 2 compartment model makes no such assumption; therefore, blood is considered a separate compartment. The myocardial tissue can be further modeled by subcompartments, creating a 3-compartment model with additional compartments representing the interstitial and intracellular space. These additional compartments are often difficult to model and often are not needed for accurate MBF determination. Time activity curves are commonly derived by dynamic region of interest sampling over the myocardium and the LV. The detailed description of compartmental modeling is beyond the scope of this review, and a more detailed description can be found elsewhere.[23]

Quantification of Flow by PET

PET is the most studied noninvasive imaging modality for the quantification of MBF, with almost 30 years of experience using ^{15}O-water, ^{13}N-ammonia, and Rubidium-82 (^{82}Rb) for blood flow quantification. The uptake of the currently used PET tracers can be modeled by 1, 2, or 3 tissue compartmental modeling. MBF (mL/min per gram) is calculated from k1 with additional correction for tracer extraction (E) in the myocardium (MBF=k1×E). Alternatively, a simplified retention model can be applied using the data acquired during early phase of imaging. This model is based on the assumption that the washout and the metabolism of the tracer is negligible at the time of early imaging; therefore, the calculation of k2 and k3 are not necessary. This simplification omits the complicated curve fitting process, which is required in the compartmental modeling for the calculation of k1, making this approach potentially more suitable for widespread routine clinical application.

^{15}O-water is the prototypical ideal perfusion agent for dynamic imaging, being freely diffusible with an almost 100% first-pass extraction. Therefore, the myocardial uptake of ^{15}O-water is highly proportional to myocardial flow in a wide range of coronary flows (0.4–5.8 mL/min per gram) and shows minimal roll-off at high flows.[24,25] The short half-life of ^{15}O-water allows for rapid serial imaging with relatively low overall radiation exposure. However, secondary to the rapid clearance and the short half-life, ^{15}O-water static images cannot be used for visual analysis. ^{13}N-ammonia readily diffuses across cell membranes, gets metabolically trapped in the myocardium with a high retention rate, and is rapidly cleared from the blood.[25,26] However, at higher flow rates, ^{13}N-ammonia shows a significant roll-off as metabolic trapping becomes rate limiting, and significant back diffusion emerges (Figure 3). ^{82}Rb is a potassium analog that is extracted by the heart via active transport through Na-K-ATPase. The first-pass extraction of ^{82}Rb approximates 40% to 50% at rest; however, as with other nondiffusible tracers, the extraction significantly drops with increased coronary flow rates.[27] A major advantage of ^{82}Rb is that it can be produced at the scanner by a portable generator. Therefore, there is no requirement for an on-site cyclotron. Unfortunately, of the 3 most commonly used PET tracers, ^{82}Rb shows the most significant roll-off. Figure 5 demonstrates time activity curves and representative PET images of a patient who underwent both ^{82}Rb and ^{13}N-ammonia PET imaging.[28] Newer ^{18}F-labeled myocardial perfusion radiotracers have been introduced, among which ^{18}F-flurpiridaz, a ^{18}F-labeled mitochondrial complex 1 inhibitor, has reached phase 3 clinical trials. This radiotracer shows favorable characteristics for dynamic PET imaging, having a high first-pass extraction and linearity with flow even at high stress-induced flow rates and slow washout with prolonged myocardial retention.[29,30] An early Phase II clinical trial demonstrated safety, better imaging quality, and higher sensitivity for improved

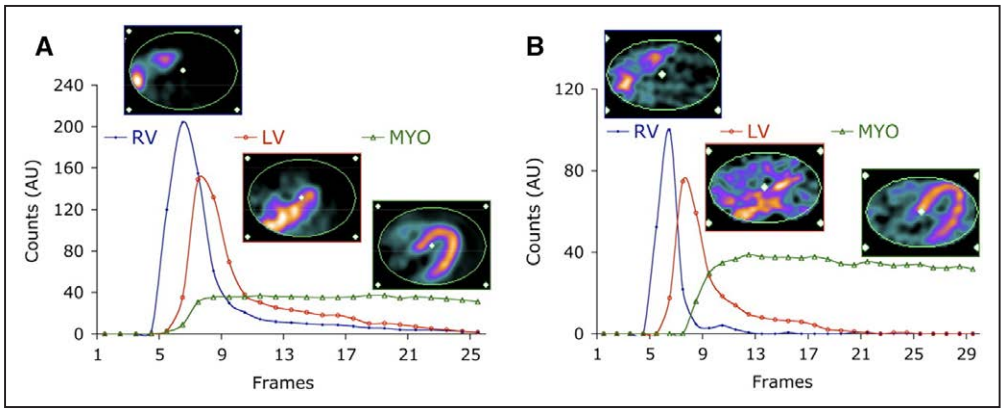

Figure 5. Illustration of kinetic modeling of positron emission tomography (PET) radiotracers. Shown are typical factors and corresponding factor images associated with ^{82}Rb (**A**) and ^{13}N-ammonia (**B**) from dynamic PET studies in same subject. AU indicates arbitrary units; LV, left ventricle; MYO, whole myocardium; and RV, right ventricle. This research was originally published in *JNM*. Reprinted from El Fakhri et al[28] with permission of the publisher. Copyright ©2009, the Society of Nuclear Medicine and Molecular Imaging, Inc.

detection of CAD when compared with ^{99m}Tc SPECT imaging.[31] The tracer is cyclotron produced, although has a longer half-life of 2 hours that allows for distribution from a regional production center, as well as facilitating imaging with exercise stress. The lower positron range of ^{18}F in comparison to other PET tracers results in excellent spatial resolution. In the first completed phase 3 trial, ^{18}F-flurpiridaz was demonstrated to be superior to SPECT for diagnosing CAD, particularly in women, obese subjects, and patients with multivessel disease.[32]

Dynamic PET myocardial imaging has been validated by microsphere blood flow studies in preclinical animal models for the absolute quantification of MBF and CFR and has been shown to be highly reproducible over a wide range of flows (0.5–6 mL/g per minute).[24,25,33] In PET imaging, attenuation correction is the cornerstone of accurate measurement of tracer uptake, which has been achieved initially with rotating attenuation line sources and more recently with CT-based attenuation correction after the introduction of hybrid PET/CT systems. The accuracy of magnetic resonance–based attenuation correction of PET using hybrid PET/magnetic resonance systems remains under active investigation. PET offers enhanced image quality because of higher count rates and better spatial resolution in addition to the routine availability of robust attenuation correction when compared with SPECT. Additionally, PET tracers usually permit lower radiation exposure than SPECT perfusion tracers mostly driven by their shorter half-life. More importantly, some of the available PET tracers (ie, ^{15}O-water, ^{13}N-ammonia) track flows better at high MBF values when compared with the commonly used ^{99m}Tc-labeled SPECT tracers. However, the relative high cost associated with PET imaging has limited widespread clinical application because of the requirement of either onsite/nearby cyclotrons or expensive generators. However, the availability of Food and Drug Administration–approved automated software packages for kinetic modeling and quantitative analysis of flow has made routine assessment of MBF and CFR feasible in the everyday clinical setting. A high agreement of global and regional MBF values across multiple software packages has been demonstrated when the same kinetic modeling was applied.[34] The growing number of installed PET scanners throughout the world has made this modality even more accessible.

Quantification of Flow by SPECT

At the present time, most of MPI is performed on SPECT imaging systems, with the number of cardiac SPECT studies significantly outnumbering the number of PET imaging studies by 10-fold. Initial attempts to quantify blood flow with conventional SPECT cameras met with mixed results; however, the recent advent of dedicated ultrafast high-sensitivity cardiac cameras capable of dynamic list mode acquisition has prompted a renewed interest in the use of dynamic SPECT for quantification of coronary flow.

The most commonly used SPECT perfusion radiotracers contain ^{99m}Tc (^{99m}Tc-sestamibi and ^{99m}Tc-tetrofosmin), characterized by 6-hour half-life and a 140 keV photon peak. However, both of these ^{99m}Tc-labeled radiotracers have relatively low first-pass extraction, show significant roll-off of radiotracer uptake at higher flow rates, and have significant liver uptake, which potentially limits their use for quantification of MBF.[35–37] In contrast, ^{99m}Tc-Teboroxime, a Food and Drug Administration–approved, radiotracer has a higher first-pass extraction and demonstrates linear uptake with flow even at higher flow rates induced by vasodilator stress. However, the rapid myocardial washout kinetics of ^{99m}Tc-Teboroxime resulted in short myocardial retention times, which along with significant lung uptake limited clinical use of this SPECT radiotracer.[38] Thallium-201 (^{201}Tl), an alternative SPECT radiotracer introduced in the 1970s, has also been applied in dynamic SPECT imaging for quantification of myocardial flow.[39] ^{201}Tl resembles potassium and is extracted by the myocardium through Na/K ATPase and has a high first-pass extraction rate. However, this radiotracer demonstrates significant redistribution, which is characterized by differential clearance from normal and ischemic myocardium based on both differences in flow and tissue viability. This property of redistribution allowed for imaging after a single injection of radiotracer and comparison of early and delayed images for the classification of myocardial regions as normal, ischemic (reversible defect), or infarcted (fixed defect). However, the relative low energy of the emitted photon (60–80 keV) along

with a particularly long half-life (73 hours) made the use of ^{201}Tl less ideal for quantitative assessment of myocardial flow.[37,40] Recently, radioactive iodinated rotenone derivatives (^{123}I-ZIROT; ^{123}I-CMICE-013) have shown great promise for dynamic SPECT MPI.[41,42] These tracers, similarly to the PET tracer ^{18}F-flurpiridaz, target mitochondrial complex-1 of the electron transport chain and demonstrate a high extraction fraction and high correlation of myocardial uptake with microsphere flow even at higher flow rates.[41,42]

Because of technical limitations related to camera sensitivity and insufficient temporal resolution, early studies using conventional cameras with NaI detectors attempting to quantify MBF by SPECT applied first-pass planar imaging using right pulmonary artery counts for arterial input functions. However, this method carried several limitations and did not allow for scatter, partial volume, and attenuation correction or permit estimates of regional MBF. More recently, newer dedicated cardiac SPECT systems equipped with stationary solid-state cadmium–zinc–telluride detectors with improved sensitivity and spatial and energy resolution have been applied for the determination of myocardial flow.[37] Preclinical validation studies evaluating a dynamic SPECT imaging protocol using a cadmium–zinc–telluride camera suggested that ^{201}Tl outperformed the ^{99m}Tc-labeled tracers based on the improved physiological properties of ^{201}Tl.[37]

Despite the recent advances in dynamic SPECT imaging, there are a handful of technical issues preventing the widespread use of SPECT for routine quantitative perfusion imaging.[43] The prerequisite of accurate quantitative estimation of myocardial flow through kinetic modeling is to obtain accurate reconstructions from the 3-dimensional SPECT data sets. At early time points, the blurring from cardiac and respiratory motion can result in overestimation of myocardial tracer uptake and underestimation of input-derived blood pool tracer concentration, whereas at later time points, the myocardial uptake can be underestimated and the blood pool overestimated. The use of dual respiratory and cardiac gating during the SPECT acquisition may resolve this issue.[43] One also needs to correct for confounding physical issues associated with SPECT imaging, including attenuation, scatter, projection truncation, and partial volume effects. Attenuation correction is now generally achieved using a low-dose CT scan for the generation of nonuniform attenuation maps. Co-registration of a contrast CT scan can facilitate anatomic colocalization of myocardial surfaces for partial volume effect correction. The typical voxel-based partial volume correction methods can increase image noise, which can be particularly important in dynamic imaging, often having low signal to noise ratio at certain time points of the time activity curve. As gamma photons cross the human body, they can also interact with the tissue in a way that results in deflection of the photon with and without energy loss (Compton or Rayleigh scattering, respectively). Scatter results in blurring and haziness of projections reduces contrast on reconstructed images and adds uncertainty in the quantification of the underlying activity distribution. In addition, radioactivity in adjacent organs or background may be truncated, and this truncation may cause quantitative errors without correction (projection truncation). Incorporating the body contour obtained from low-dose CT from hybrid systems or coregistered CT images in reconstruction have been shown to provide the most accurate flow estimates in dynamic SPECT studies.[37] Of note, in comparison to PET, where correction for scatter and attenuation is always performed, these are not routinely done for dynamic SPECT imaging studies, and studies without these critical corrections require careful interpretation.

Quantification of Flow by CT

With the advent of new multidetector CT technology with state of the art 128, 256, and 320 detector rows, coverage of the entire heart became possible with only one gentry rotation. This provided feasibility of adequate serial myocardial and blood pool sampling for the true quantification of MBF. Dynamic CT scanning is performed after injection of a contrast agent with prospective ECG triggering of each scan at frequent intervals (every or every other heartbeat) for ≈30 seconds after contrast administration to recover the first pass of the contrast medium. From these dynamic image sets, myocardial and arterial input time activity curves can be generated and then mathematical modeling can be applied to produce estimates of absolute myocardial flow. Because CT contrast agents are similar in characteristics compared with magnetic resonance imaging (MRI) contrast agents (low molecular weight, free diffusion across capillary membranes, no intracellular uptake), mathematical models previously used for MRI flow quantification have been successfully adapted for dynamic CT flow calculation. The most frequently used methods include upslope analysis, model-based deconvolution technique, and Patlak plot analysis.

The iodinated contrast agents that are currently used clinically are nonionic, have relatively high iodine concentration, and can be iso-osmolar or have low-osmolality. Notably, these iodinated contrast agents can influence coronary physiology. Tatineni et al[44] has shown that iodinated contrast agents induce coronary vasodilation that is comparable to the vasodilation induced by nitroglycerin. Unlike purely intravascular particulate emulsion contrasts, conventional nonionic contrast agents significantly diffuse to the extravascular space during the first passage, and thereby, they tend to overestimate IMBV.[45] The first-pass extraction of nonionic contrasts is estimated to be at 33% at hyperemic flow conditions in nonstenotic vessels and significantly higher (50%) in ischemic coronary territories.[45] Unlike gadolinium-based MRI contrast materials, iodinated CT contrast agents show linear relationship between contrast concentration and enhancement.

The major advantages of CT MPI are the superior spatial resolution of CT and the relative cost-effectiveness of the technique. CT provides the opportunity to perform accurate anatomic and functional assessment of both the myocardium and the coronary circulation within one examination, providing invaluable luminal and extraluminal structural information about the epicardial coronary arteries as well. As mentioned earlier, with dynamic CT imaging, the IMBV can be calculated and may provide additional information about the coronary microcirculation. State-of-the-art CT scanners have sufficient spatial resolution to enable differentiation between the endocardium and the epicardium, and the attenuation difference between these 2 layers (especially when assessed

during rest and stress conditions) can provide unique information about the microcirculation, more specifically decreased endocardial over epicardial contrast ratios, and associated CT attenuation values have been associated with microvascular abnormalities.[46] Another advantage of CT perfusion imaging is the possibility to calculate linear spatial variations in iodine concentration along the vessel (transluminal attenuation gradient).[18] There is also the possibility to derive estimates of regional myocardial perfusion associated with each coronary artery territory using computational modeling of the contrast within the large vessels.[19,47]

However, all these benefits potentially come at a price of higher radiation; even with prospective gating, a combined rest and stress dynamic study exposes patients to as much as 15 to 20 mSv radiation. The availability of new CT scanners that operate at lower kVp, with advanced iterative reconstructions, and the application of newer acquisition protocols and quantitative approaches have the potential to significantly reduce the radiation exposure. In light of newer studies showing improved accuracy of hyperemic MBF above CFR,[48] in the future, the radiation dose might be further lowered by limiting studies to stress only imaging. However, some issues will remain of concern. For example, with dynamic CT imaging, the image quality might be compromised at stress by the increased heart rate, introducing motion artifacts. Beam hardening artifacts arising from high attenuation contrast agents or coronary calcium can also affect image quality, although image-based beam hardening correction has been shown to improve CT-derived coronary flow accuracy by microsphere flow.[49] Dual-energy CT provides another means for overcoming calcium-related beam hardening during CT MPI.[50] Because contrast agents are not without physiological effects in the coronary circulation, baseline flow measurements might be overestimated, and this could lead to underestimation of CFR. Contrast-induced nephropathy is also a feared complication of CT angiography; therefore, patients with baseline renal disease are usually excluded from these studies. Figure 6 depicts color maps for MBF and IMBV in a patient who underwent dynamic CT imaging.[51]

Quantification of Flow by MRI

The high spatial and temporal resolution of MRI (particularly with 3 Tesla scanners) combined with the lack of radiation makes MRI an excellent tool for estimation of MBF. After the injection of gadolinium-based contrast agents, first-pass imaging of the myocardium is performed, based on the T1 relaxation shortening properties of gadolinium. Well-perfused myocardium has shorter T1 and appears bright on heavily T1-weighted images. First-pass images obtained with dynamic contrast MRI have been routinely evaluated for the assessment of MBF by visual assessment or by semiquantitative approaches, such as quantitative analysis of the upslope in regional myocardial contrast intensity. True MBF quantification requires rapid repeated acquisitions (such as fast low-angle shot, echo planar imaging, or steady-state free precession imaging) at multiple short-axis locations. These techniques are often combined with parallel imaging techniques with the goal of reducing acquisition time. To maintain adequate temporal sampling, the number of short-axis slices is usually restricted to 3 to 4 slices. Blood pool signal intensity is recorded as a reference.

The gadolinium chelates that are currently used clinically as MRI contrast agents have a low molecular weight and freely diffuse across capillary membranes into the extracellular space without any substantial intracellular uptake. Importantly, the gadolinium concentration is only linear with signal intensity at lower concentrations and at higher doses (gadolinium concentration >4 mmol/L, often used in nonquantitative perfusion imaging for better visualization of perfusion defects) result in signal saturation that can lead to inaccurate estimation of MBF.[52] To avoid signal saturation during the early dynamic imaging phase, a dual bolus imaging has been applied. In this approach, a lower bolus is administered for determination of the arterial input curve, which is followed by a higher bolus with a repeat acquisition for visualization and quantification of the myocardial phase.[53,54]

Using the measured arterial input function and the tissue signal intensity, time intensity curves are constructed and kinetic modeling applied to quantify MBF. The most widely applied modeling techniques quantify MBF via compartmental kinetic modeling (Patlak plot, modified Kety equitation) or by deconvolution methods (Fermi deconvolution, model-independent deconvolution, exponential basis deconvolution, and B-spline basis deconvolution). The Patlak plot method enables the calculation of the k1 transfer constant by linear least-squares fitting, simplifying the analytic approach to a 2-tissue compartment model.[55] It only includes data from the early phase of contrast arrival when the extracellular contrast concentration is not substantial enough to cause back diffusion into the intravascular space. The k1 in this case represents the 1-way transfer of gadolinium containing contrast material from the LV blood pool to the myocardium. The main weakness of this compartmental modeling approach is that MBF is calculated as K1 divided by the extraction fraction, and there is a nonlinear decrease in the extraction of gadolinium contrast agents with increasing flow. Deconvolution methods model contrast enhancement using a linear time invariant system, calculating the myocardial impulse by deconvolution of the measured tissue response with the arterial input function.[56] The Fermi model, which was initially developed for purely intravascular contrast agent studies, can also be applied for MBF calculations for extravasating tracers as long as the intravascular tracer concentration stays significantly higher than the extravascular concentration (eg, during first-pass diffusion).[57] B-spline basis deconvolution uses the degree and number of splines and the position of the break points to calculate MBF, whereas the total number of exponential functions and decay rate of the exponential functions are the parameters in exponential basis deconvolution.[56] The model-independent deconvolution method applies sophisticated mathematical technique for input response function calculation.[58] A recent MRI study performing head-to-head comparison of 4 different mathematical modeling applications (Fermi model, uptake model, 1-compartmental model, model-independent deconvolution) concluded that there was no difference in diagnostic performance.[59]

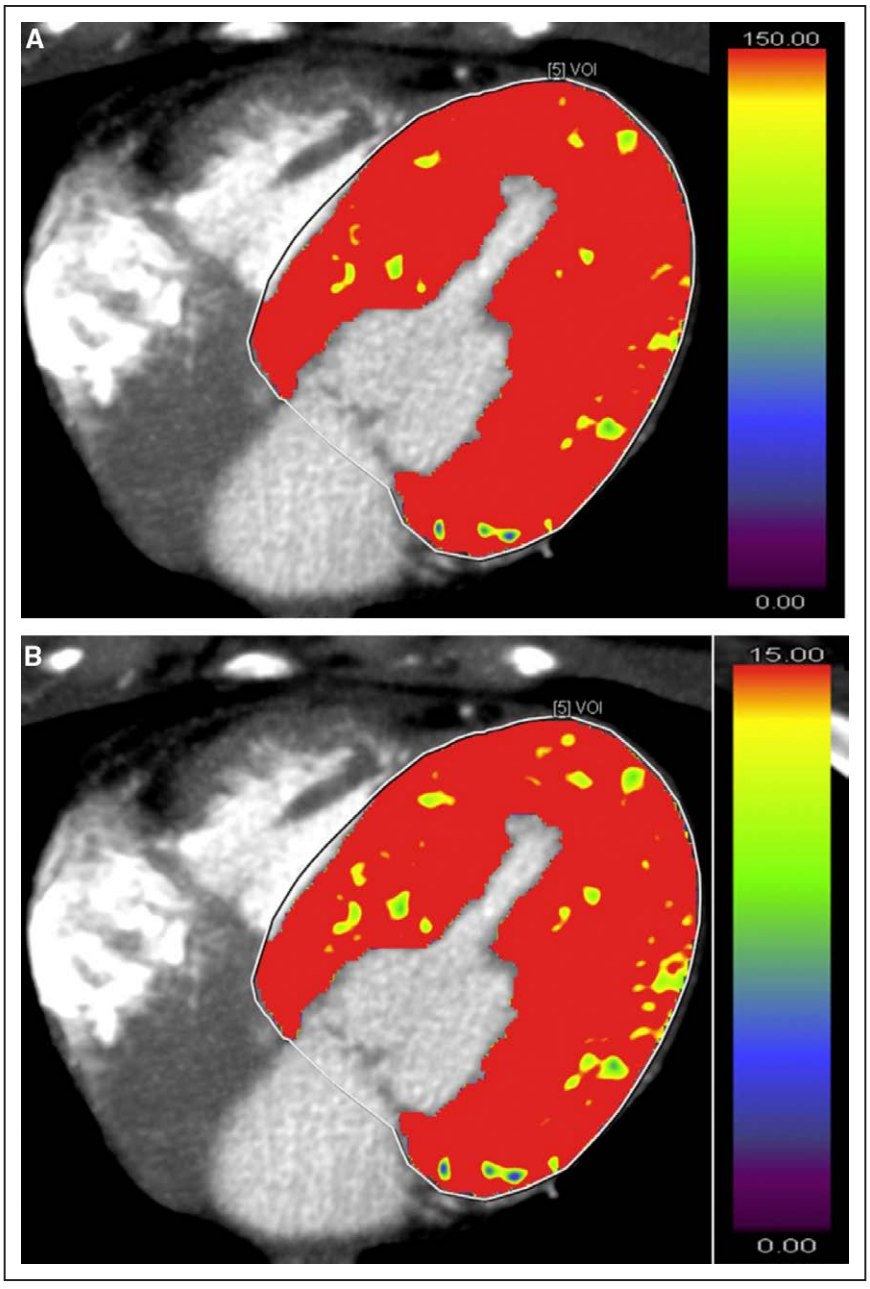

Figure 6. Computed tomography (CT) perfusion imaging of a patient who underwent dynamic contrast CT imaging for suspected coronary artery disease. No visual perfusion defect was detected. **A** and **B**, The color maps for myocardial blood flow and myocardial blood volume, respectively. Global left ventricular myocardial blood flow and volume were 157.7 mL/100 mL/min and 19.3 mL/100 mL, respectively. Adapted from Vliegenthart et al[51] with permission of the publisher. Copyright ©2016, Society of Cardiovascular Computed Tomography.

When applying MRI for evaluation of MPI, there needs to be a consideration of artifacts. Subendocardial dark artifacts (dark-rim artifact) can transiently appear on contrast-enhanced MRI images at the time when the gadolinium contrast reaches the LV blood pool. This not only affects visual image analysis, but the artifact can induce significant differences in the estimation of MBF by either changing the contrast upslope or baseline for signal difference calculations or changing the fit parameters of a compartment model or a nonmodel-based approach. The dark rim is likely multifactorial in origin, caused by Gibbs ringing–related resolution limitation and cardiac motion effects.[60] Besides the aforementioned nonlinear relationship of contrast enhancement and contrast concentration, the main disadvantages of quantitative MRI perfusion imaging are the relatively complicated postacquisition processing and the relatively higher cost. Gadolinium contrast agents are also contraindicated in patients with advanced renal failure, and this approach should not be used when the glomerular filtration rate is <30.

MRI-derived MBF has been shown to correlate well with microsphere-derived MBF in animal models.[57,58] The advantages of MRI are the high spatial resolution allowing transmural MBF characterization and the lack of ionizing radiation, along with the ability to perform a more comprehensive cardiovascular assessment of structure and mechanical function. MRI has also been used to accurately quantify IMBV using first-pass perfusion. Additionally, T1 mapping at rest and during adenosine stress has been recently demonstrated to be able to differentiate between normal, infarcted, ischemic, and remote myocardium with distinctive T1 profiles.[61] Figure 7 shows images of a quantitative myocardial perfusion MRI study of a patient diagnosed with hypertrophic obstructive cardiomyopathy.[62]

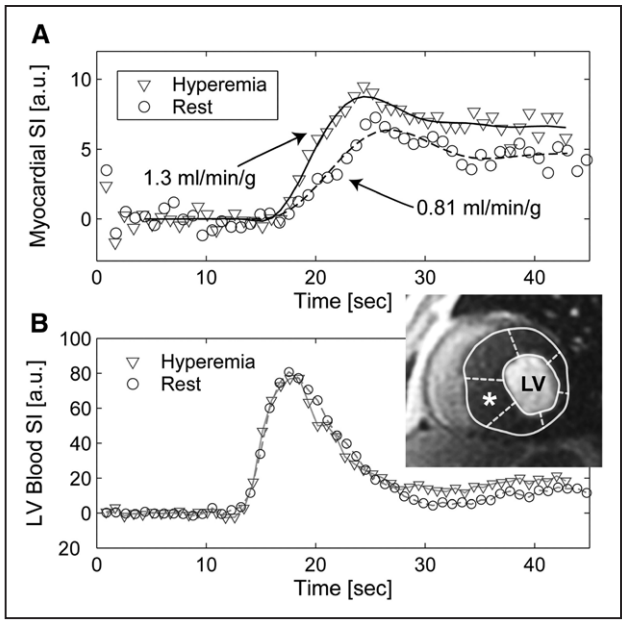

Figure 7. Quantitative magnetic resonance imaging (MRI) myocardial perfusion at rest and during adenosine in a 31-year-old male patient with hypertrophic obstructive cardiomyopathy. **Top**, The signal intensity (SI) curves (in arbitrary units [AU]) during the first pass of a contrast agent bolus in the hypertrophied basal myocardial segment (marked as *). **Bottom**, The SI curves in the blood pool used as the arterial input function. LV indicates left ventricle. Adapted from Petersen et al[62] with permission of the publisher. Copyright ©2007, The American Heart Association, Inc.

Quantification of Flow by MCE

MCE has been validated for the quantification of absolute MBF and determination of IMBV.[12,63] The most clinically used ultrasound contrast agents consist of gas containing microbubbles that have a shell composed of lipid, albumin, or biopolymers filled with perfluoropropane or sulfur hexafluoride gas. These microbubbles are generally 1 to 8 μm in diameter and resemble red blood cells with regard to size and rheological properties. They can pass through the capillary network, although remain stable in the circulation as imageable intravascular contrast agents. These gas-filled microbubbles expand and contract (resonate) in response to acoustic waves, producing a detectable signal distinct from tissue. When delivered as a constant intravenous infusion, they achieve a steady-state concentration, however, can be locally destroyed in the myocardium with the delivery of high-intensity acoustic signals (mechanical index >0.5). Pioneering work by Kaul et al established an approach for quantification of myocardial flow using MCE (Figure 8).[12] The monitoring of the rate of myocardial replenishment by microbubbles postdestruction can be used to generate time–acoustic intensity curves. The changes in signal intensity over time are fit to an exponential function, with peak signal intensity reflecting the IMBV and the rate of appearance of contrast reflecting the flow velocity in the microcirculation. The product of these 2 parameters has been shown to equate to MBF.[12] The MCE approach has been used to evaluate cycle-dependent change in IMBV as an index of stenosis severity[64,65] and the changes in flow and IMBV during pharmacological stress.[66]

The quantification of flow with MCE has been validated in preclinical studies against microspheres, and MCE has been shown to provide a good correlation with PET-derived MBF in humans.[12,63] MCE has been extensively used in post-PCI imaging for detecting flow-limiting microvascular obstruction (no-reflow phenomenon).[67] The major advantages of MCE against some of the other dynamic imaging modalities is the lack of ionizing radiation, the wide availability, and relative inexpensiveness of this technology. Recently, drug-coated microbubbles have been used for intravascular tissue–targeted imaging of angiogenesis and transplant rejection, as well as for gene or targeted drug delivery.[68] Regarding potential disadvantages, the techniques used with MCE are operator-dependent. In particular, maintaining the image plane during replenishment of microbubbles is crucial to get an accurate estimation of flow. Obesity, respiratory motion, and parenchymal lung diseases can also result in suboptimal MCE images. High concentration of microbubbles in the near field can cause attenuation of a significant proportion of the ultrasound, which can lead to failure to opacify and adequately assess the far field. Microbubble destruction in the near field can also result in swirling artifacts.

Molecular Imaging and Coronary Flow

In noninvasive imaging, there is increasing demand for the development of molecular and cell-specific probes to visualize and characterize subcellular biological processes. Recent advancements in instrumentation, imaging technology, and molecule/cell-specific tracer development enhanced progress in the last few decades; therefore, many modalities used for quantification of myocardial flow (PET, SPECT, MCE, and MRI) can be used for targeted molecular imaging. Specific probes have been developed to image angiogenesis, myocardial metabolism and remodeling, cardiac neuroreceptors, atherosclerosis, and inflammation.[68] Activation of the sympathetic nervous system initiates vasodilatation in the coronary resistance vessels and, thereby, increases MBF via an endothelium-dependent mechanism. Reductions in MBF have been correlated with sympathetic denervation in multiple disease processes associated with CMVD, including diabetes mellitus,[69] and primary CMVD.[70] Sympathetic imaging has also been used in cardiac transplant patients to demonstrate regional differences in the reinnervation of the transplanted heart, which correlated well with impaired MBF responses to CPT and endothelium-dependent vasodilation.[71] Myocardial metabolism is closely coupled with blood flow because of the high resting oxygen extraction, and therefore, any rise in oxygen demand has to be matched with an increase in MBF. ^{11}C-acetate can be used for the estimation of myocardial oxygen consumption, and based on the high first-pass extraction, the agent has also been used for quantification of MBF.[72] Although ^{11}C-acetate has provided an estimation of myocardial flow comparable to that of ^{13}N-ammonia, the use of this agent has not gained widespread utilization, possibly related to the complexity of producing ^{11}C-labeled tracers. Myocardial ^{18}F-fluorodeoxyglucose imaging in conjunction with quantification of myocardial flow has been used to predict improvement in global and regional LV function in response to revascularization for over 30 years.[73] As inflammatory cells

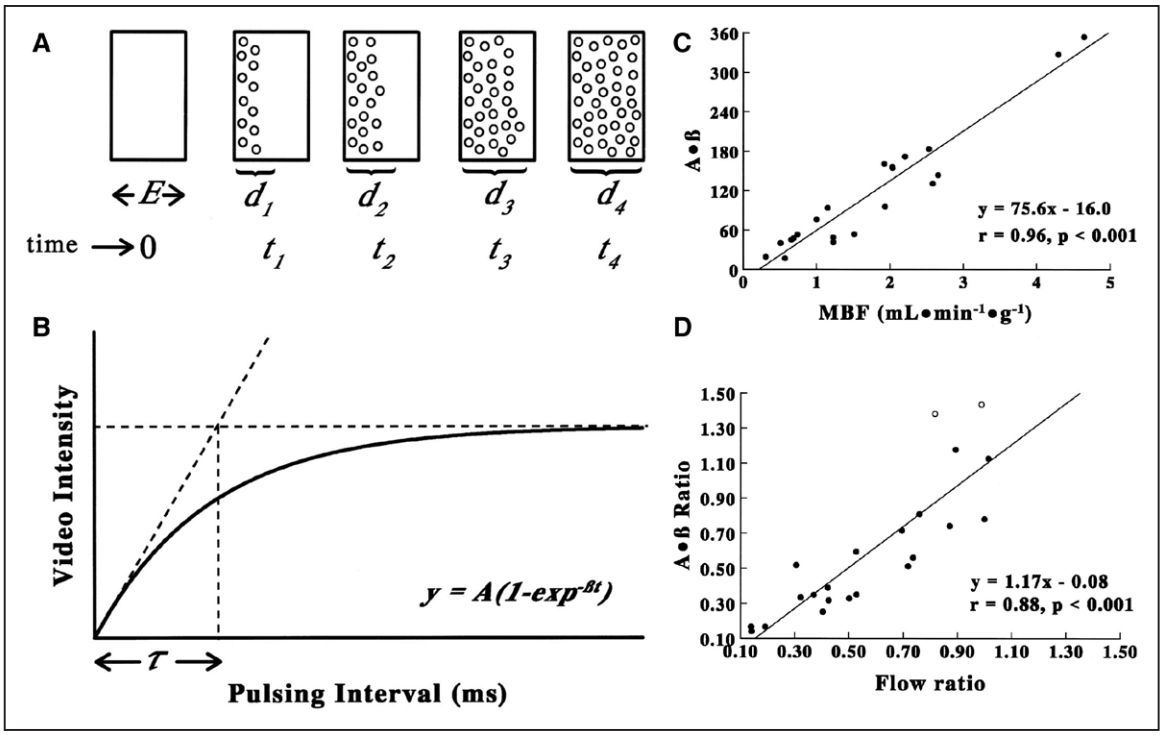

Figure 8. Contrast echocardiography for assessment of flow and intramyocardial blood volume. Microbubbles are delivered as a constant infusion and myocardial contrast echocardiography performed using different pulsing intervals. **A**, The elevation (thickness) of the ultrasound beam is represented as *E*. If all the microbubbles in the elevation are destroyed by a single pulse of ultrasound at t_0, then replenishment of the beam elevation (d_1 through d_4) will depend on the velocity of microbubbles and the ultrasound pulse interval *t*. **B**, The relationship between video intensity (*y* axis) and pulsing interval (*x* axis) are plotted. When the pulse interval exceeds *T*, the video intensity will remain constant. This plateau phase will reflect the effective microbubble concentration within the myocardial microcirculation. The myocardial video intensity versus pulsing interval plots are fitted to an exponential function: $y = A(1 - e^{-\beta t})$, where *A* is the plateau video intensity reflecting the microvascular cross-sectional area, and β reflects the rate of rise of video intensity and, hence, microbubble velocity. In acute preclinical validation studies, excellent correlations were found between microsphere flow and β, as well as flow and the product of *A* and β. **C**, A relationship between radiolabeled microsphere–derived myocardial blood flow (*x* axis) and $A \times \beta$ derived on MCE (*y* axis) in experimental animals after intracoronary delivery of a vasodilator. **D**, The relation between the ratio of radiolabeled microsphere–derived myocardial blood flow from the stenotic and nonstenotic beds (*x* axis) and the $A \times \beta$ ratio derived on MCE from the stenotic and nonstenotic territory (*y* axis) in another group of animals with coronary stenoses. Adapted from Wei et al[12] with permission of the publisher.

display high glycolytic activity, ^{18}F-fluorodeoxyglucose is also applied for evaluation of myocardial inflammation that occurs with infiltrative myocardial diseases. A close correlation between inflammation and regional impairment in MBF has been recently demonstrated in cardiac sarcoidosis.[74]

Assessment of CMVD in Patients Without CAD: Primary CMVD

CMVD can develop secondary to several underlying mechanisms; on the basis of clinical settings, it can be differentiated into 3 major categories: CMVD in the absence of CAD or other myocardial disease (primary CMVD), CMVD in the presence of obstructive CAD (including iatrogenic CMVD caused at the time of revascularization), and CMVD in the presence of other myocardial diseases.[1] The assessment of myocardial flow with dynamic imaging modalities reflects an integration of flow in the epicardial arteries and the microcirculation. In the absence of epicardial stenosis, any reduction in the MBF is assumed to be caused by functional or structural alterations in the coronary microcirculation causing CMVD. Cardiac catheterization reveals nonstenotic epicardial coronaries in 20% of patients with typical exertion-induced chest pain, and two third of these patients show abnormalities on invasive coronary microvascular testing.[22] Chest pain without obstructive CAD comprises multiple etiologies, including musculoskeletal, pulmonary, and psychiatric pain syndromes in addition to non-CAD cardiac pain. In certain cases, noninvasive quantification of MBF is able to differentiate noncardiac from cardiac pain by diagnosing CMVD.

Chest Pain Without Obstructive CAD

Cardiac syndrome X (CSX) is a frequently used diagnostic term for the subset of non-CAD chest pain patients, most commonly used in cases when chest pain is linked to objective evidence of ischemia during exercise electrocardiography or nuclear stress perfusion imaging; however, the diagnosis of CSX has been used liberally in the literature, with significant differences in the definitions across publications. The heterogeneity of CSX patients is highlighted by the fact that a reduced CFR is not a consistent finding in all patients with CSX; only approximately half of these patients show impaired CFR by dynamic PET.[21] Bøttcher et al[75] demonstrated with ^{13}N-ammonia PET blood flow measurements in CSX patients that despite impaired CFR during dipyridamole vasodilator

stress, the MBF response to CPT remained intact, suggesting endothelium-independent alterations in coronary flow. In this study, infusion of the nitric oxide precursor L-arginine had no influence on either the resting myocardial perfusion or the CPT-induced hyperemia. Recently, in patients with chest pain without significant obstructive CAD, CT-derived myocardial perfusion reserve was found to be progressively decreased from the epicardium to endocardium.[46] A recent study has also demonstrated an association between elevated CRP levels and reduced PET-derived CFR in CSX patients, pointing to the importance of inflammation in the pathogenesis of CSX-related chest pain.[76]

CMVD is highly prevalent in women presenting with chest pain syndromes; a reduced CFR has been reported in nearly one half of women presenting with chest pain in the absence of obstructive CAD.[77] The high prevalence in women has been hypothesized to be caused by sex differences in vasoreactivity and vascular remodeling.[78] Traditionally patients with microvascular angina were considered low risk; however, recent data indicate that the diagnosis of CMVD is associated with increased morbidity and mortality, particularly in women.[79] In the WISE study (Women's Ischemia Syndrome Evaluation) in women without obstructive CAD, a reduced CFR was found to be associated with adverse clinical outcomes at mean follow-up of 5.4 years.[80]

Current practice guidelines offer limited guidance for making the diagnosis of CMVD. In the setting of acute coronary syndrome, the American Heart Association/American College of Cardiology guidelines recommend considering invasive CFR measurement if coronary angiogram reveals nonobstructed epicardial arteries and CMVD is suspected (Class IIb; Level of Evidence B).[81] The European Society of Cardiology guidelines recommend CFR quantification by PET or transthoracic Doppler echocardiography in the LAD for the diagnosis of microvascular angina, without consensus in regards the use of MCE or MRI for quantification of MBF.[82] Once the diagnosis is established, the European Society of Cardiology recommends reassurance and symptom relief with either nitrate, β-blocker, or calcium channel blocker therapy.[82]

When impaired CFR is demonstrated on invasive testing or by noninvasive quantification of MBF in non-CAD chest pain patients, it is reasonable to assume that the angina is secondary to primary CMVD, and appropriate changes in treatment strategies can be implemented. Currently, there is little evidence that establishes the most effective treatment strategies for the treatment of primary CMVD. In addition to risk factor control and the aforementioned traditional antianginal therapies (nitrates, β-blockers, calcium channel blockers), nontraditional antiischemic drugs (nicorandil, ivabradine, and aminophylline) have been proposed for the treatment of microvascular angina.[78] A recent pilot study detected improvement in ^{82}Rb PET-derived CFR after 1 month of treatment with sodium current inhibitor ranolazine in patients presumed to have primary CMVD.[83] The promising finding of this study suggests that PET-derived CFR might serve as a tool for monitoring the response to therapy in primary CMVD patients.

Aging

Normal aging has been associated with a progressive reduction in coronary flow.[84,85] PET-derived basal and hyperemic MBF is comparable in patients ≤60 years of age; however, above the age of 60 years, basal flow increases, likely related to increase in cardiac workload generated by elevated systolic blood pressure (basal coronary flow 0.76±0.17 mL/min per gram in young versus 0.92±0.25 mL/min per gram in older patients).[84] In addition, above the age of 70 years, hyperemic flow becomes blunted as well and, therefore, further reducing PET-derived CFR (CFR: 3.54±0.96 in patients <30 years, 4.23±1.35 in patients 30–49 years, 3.51±1.21 in patients 50–69 years, and 1.94±0.46 in those >70 years).[85]

Smoking

PET-derived CFR is 21% lower in long-term asymptomatic smokers when compared with control subjects (CFR: 3.8±0.6 versus 4.6±0.9, respectively).[86] Coronary endothelial dysfunction has been demonstrated in smokers by impaired PET MBF during CPT, when compared with controls.[6] Importantly, the abnormal MBF response to CPT is normalized at 1 month after smoking cessation and remains preserved for 6 months after discontinuation of smoking.[6]

Hypertension

Reduction in PET-derived CFR has been demonstrated in patients with LV hypertrophy secondary to hypertension in the absence of epicardial CAD.[87,88] Importantly, the impairment in CFR is not correlated with LV mass.[87] This observation suggests that intrinsic microvascular abnormalities (vascular remodeling and endothelial dysfunction) may play more important role in the pathogenesis of hypertension-associated CMVD than LV hypertrophy. The blunting in CFR appears to be transmural, uniformly affecting both subendocardial and epicardial perfusion,[87] and appears to happen early in the disease process because lower hyperemic flow has been demonstrated in asymptomatic prehypertensive patients.[88] The fact that each step in the development of hypertension is associated with worsening CFR suggests that CFR may progressively worsen with the evolution of the disease (CFR: 2.91±0.53 in controls, 2.54±0.48 in prehypertensive patients, and 2.23±0.47 in hypertensive patients).[88] Additionally, improvement in hyperemic MBF has been described after treatment with oral antihypertensives.[89]

Hyperlipidemia and Obesity

Impairment in CFR has been documented by PET in asymptomatic hyperlipidemic patients with nonobstructive CAD, and the reduction in CFR has been correlated with total and low-density lipoprotein cholesterol levels.[90] Moreover, treatment of hyperlipidemic patients with fluvastatin[91] or pioglitazone[92] has been shown to improve PET-derived CFR mostly driven by improvement in hyperemic MBF. Patients with obesity without significant comorbidities have also shown blunted hyperemic MBF response on PET when compared with nonobese subjects.[7,8] Impairment in endothelium-dependent coronary vasomotion is present in overweight individuals as evidenced by impaired MBF response to CPT, which progresses to impaired vasodilator capacity to dipyridamole in obese individuals.[7] Related to these findings, bariatric surgery has been demonstrated to cause marked improvement in MBF

in morbidly obese patients after CPT (presurgery 0.93 mL/min per gram; postsurgery 1.08 mL/min per gram; P=0.03) and dipyridamole-induced hyperemia (presurgery 1.53 mL/min per gram; postsurgery 2.51 mL/min per gram; P<0.001).[8]

Diabetes Mellitus

Endothelial dysfunction is the hallmark feature of diabetes mellitus, and impaired CFR has been demonstrated in both type 1 and type 2 diabetic subjects with multiple dynamic imaging modalities, including PET,[10,93] CT,[51] and MRI.[94] In a patient cohort referred for cardiac stress/rest PET imaging, those patients with diabetes mellitus and impaired CFR (CFR<1.6) showed yearly cardiovascular death rate comparable to nondiabetic patients with known CAD (2.8% versus 2.0%, respectively), whereas those diabetic patients with preserved CFR had yearly cardiac death rate comparable to patients without diabetes mellitus and without CAD (0.3% versus 0.5%; Figure 9).[93] Based on these findings, the authors postulated that diabetic patients with diffuse epicardial atherosclerosis or CMVD may carry a prognosis comparable to those with obstructive epicardial disease. There is limited evidence suggesting that quantification of MBF using dynamic imaging may be able to capture the early and progressive impairment of CFR at various stages of insulin resistance.[10] Compared with controls, insulin resistance alone was associated with impaired endothelial function as evidenced by a blunted MBF response to CPT. In this study, in addition to impaired MBF with CPT, CFR was also impaired during adenosine stress in patients with overt diabetes mellitus, suggesting an impairment in endothelium-independent vasodilation. CFR was even further reduced in patients with concomitant hypertension. The impairment in MBF with CPT in diabetics has been correlated with the extent of sympathetic nerve dysfunction, as determined by reduced ^{11}C-hydroxyephedrine retention.[69]

Assessment of CMVD in Presence of Obstructive CAD

Impaired hyperemic flow and CFR can be detected in patients with known single-vessel CAD even in coronary territories not affected by obstructive stenosis,[95] and alterations in myocardial flow can be observed in coronary territories with atherosclerotic disease well before the development of hemodynamically significant luminal narrowing.[5] It has been postulated that the impaired CFR in this instance could be explained by (1) early atherosclerotic disease evidenced by structural alterations (eg, increased calcium content) in the epicardial coronary wall affecting the coronary microcirculation or (2) diffuse atherosclerotic involvement of epicardial vessels.[5,96] The former hypothesis is supported by imaging studies that confirm the presence of perfusion abnormalities in patients with traditional atherosclerotic risk factors in the absence of obstructive CAD.[51,86,90,93,94]

Integrating quantitative noninvasive flow parameters with qualitative MPI provides superior diagnostic accuracy for the diagnosis of CAD than MPI alone and offers incremental risk stratification in CAD patients.[97] The value of CFR is highlighted by a recent study investigating 2783 consecutive patients referred for PET stress perfusion imaging, which identified impaired CFR (<2.0) to be associated with a 2- to 3-fold increase in cardiovascular death and increased adverse events, whereas severely reduced CFR (<1.5) was associated with a 6-fold rise in the risk of cardiac death.[97] Using absolute MBF quantification in addition to conventional MPI can be especially beneficial in patients with triple-vessel disease for whom relative coronary perfusion assessment may fall short to uncover ischemia because of balanced hypoperfusion. Recently, it has been demonstrated that evaluation of stress MBF may perform better than noninvasive assessment of CFR in the detection of flow-limiting CAD, implying that stress-only protocols may be sufficient for diagnostic stress imaging studies.[48] Also emerging evidence suggests that hybrid imaging techniques (particularly PET/CT) capable of obtaining both anatomic and functional information about the coronary vasculature might be able to separate microvascular dysfunction (reduced CFR, normal epicardial anatomy) from obstructive CAD (reduced CFR and epicardial stenosis) at the expense of increased radiation exposure.[48] However, with advent of high-sensitivity 3-dimensional PET ^{82}Rb perfusion

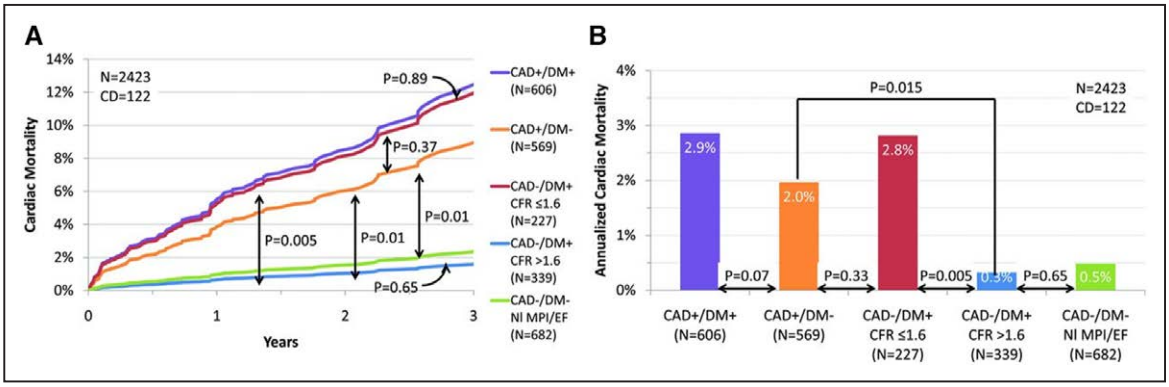

Figure 9. Annualized cardiac mortality among patients with diabetes mellitus (DM) or coronary artery disease (CAD). Adjusted cardiac mortality among patients with CAD (ie, history of coronary revascularization or myocardial infarction) without DM (orange), DM patients without CAD who have impaired coronary flow reserve (CFR; red), DM patients without CAD who have preserved CFR (blue), and patients without DM or CAD with normal scans (no scar, ischemia, or left ventricular dysfunction; green) presented as survival curves (**A**) and annualized cardiac mortality rates (**B**). Data for patients with CAD and DM are also presented for comparison (purple). CD indicates cardiac death; EF, ejection fraction; and NI MPI, normal myocardial perfusion imaging. Adapted from Murthy et al[93] with permission of the publisher.

imaging with low dose prospective ECG-gated CT angiography and the use of stress-only imaging, the radiation exposure would be fairly low (potentially <3 mSV).

It is important to note that a reduction in CFR can occur with both obstructive CAD and impairment in coronary microvascular function. Differentiating the patients with true obstructive CAD (who could benefit from revascularization) from patients with predominantly microvascular disease remains a debated topic and a major challenge in routine clinical practice. Large randomized trials reported that intracoronary pressure–based FFR-driven revascularization was associated with better outcomes when compared with angiographic severity–guided PCI or medical treatment alone; however, the net benefit was mostly driven by urgent revascularization and not by a reduction in the rate of mortality or myocardial infarction.[98] Despite the relatively similar diagnostic accuracy of FFR and CFR, studies have surprisingly reported poor correlation between FFR and invasive or noninvasive CFR; discordance between these values can be found in 30% of the cases (Figure 10).[99] Based on the concordance/discordance of FFR and CFR, measurements can be grouped into 4 distinct categories: (1) concordant normal values indicate nonobstructive coronary anatomy and normal coronary microvascular physiology, (2) concordant abnormal FFR and CFR indicate obstructive disease with reduced downstream MBF, (3) normal CFR and reduced FFR reflects predominantly focal, but nonflow-limiting epicardial disease, and (4) reduced CFR and normal FFR have been postulated to have predominant CMVD or diffuse coronary atherosclerotic involvement. Interestingly, when compared with concordant normal results, normal FFR with abnormal CFR has been associated with increased risk of major adverse events, whereas normal CFR and reduced FFR showed no increased risk.[99] This highlights the importance of CMVD or diffuse atherosclerotic disease on cardiovascular outcomes.

Differentiating between focal/diffuse CAD and CMVD can be very challenging; several invasive and noninvasive diagnostic tools have been applied to separate these entities (Figure 11 and Table 1) Invasive quantification of resistance can be useful because microvascular resistance is not affected by epicardial stenosis when collateral coronary flow is taken into consideration, but it requires invasive left heart catheterization. FFR and CT-FFR are indicators of focal stenosis, with ample evidence showing their routine applicability for differentiating mild nonflow-limiting stenosis from severe stenosis.[98] A small (10 mm Hg) pressure gradient has been observed in diffuse atherosclerotic disease, which still translates to nonstenotic FFR.[100] Secondary to microvascular compensatory mechanisms, baseline MBF remains preserved up to relatively late stage of atherosclerotic disease, however, is reduced in the presence of severe stenosis. As hyperemic flow becomes compromised in the presence of both an epicardial stenosis and CMVD, despite being a useful marker for disease severity and outcome, CFR usually cannot completely discriminate between CMVD and diffuse or obstructive CAD. Therefore, a normal-appearing coronary angiogram linked with reduced CFR could represent both diffuse atherosclerotic disease and CMVD. When invasive microvascular resistance indices are not available, IMBV and transluminal attenuation gradient

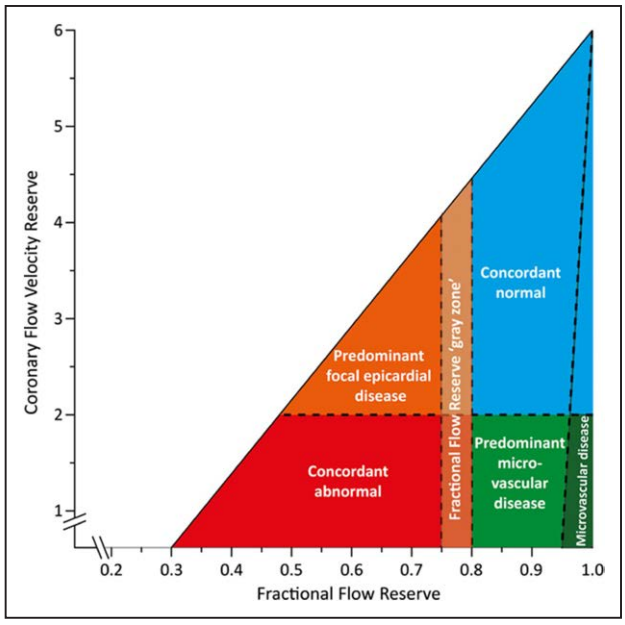

Figure 10. Conceptual plot of the fractional flow reserve (FFR)–coronary flow velocity reserve (CFVR) relationship. Four main quadrants can be identified by applying the clinically applicable cutoff values for FFR and CFVR, indicated by the dotted lines. Patients in the upper right blue area are characterized by concordantly normal FFR and CFVR, and patients in the red lower left area are characterized by concordantly abnormal FFR and CFVR. Patients in the upper left orange area and lower right light green area are characterized by discordant results between FFR and CFVR, where the combination of an abnormal FFR and a normal CFVR indicates predominant focal epicardial, but nonflow-limiting, coronary artery disease, and the combination of a normal FFR and an abnormal CFVR indicates predominant microvascular involvement in coronary artery disease. The small dark green region in the lower right is characterized by an FFR near 1 and an abnormal CFVR, indicating sole involvement of the coronary microvasculature. The FFR gray zone indicates the equivocal 0.75 to 0.80 FFR range. Adapted from van de Hoef et al[99] with permission of the publisher. Copyright ©2014, The American Heart Association, Inc.

can provide potential means of differentiation between these 2 entities. Diffuse atherosclerotic disease is associated with compensatory increase in IMBV and a gradually decreasing transluminal attenuation of contrast material, while CMVD is associated with marked reduction in IMBV and normal luminal contrast attenuation.

Impaired CFR has been also observed in acute coronary syndrome patients after successful thrombolysis or catheter-based revascularization.[101,102] This type of microvascular injury is often categorized as iatrogenic CMVD (also called coronary no reflow or microvascular obstruction) and is primarily caused by arteriolar vasoconstriction or microvascular embolization of atherosclerotic debris.[67] The presence of iatrogenic CMVD has been closely associated with poor cardiovascular outcomes, and pharmacological treatment with intracoronary vasodilators have been successfully applied to alleviate the disruption in microvascular function.[67]

CMVD in Other Cardiac Diseases

CMVD has been identified in multiple cardiac diseases, which directly or indirectly alter the myocardium and coronary

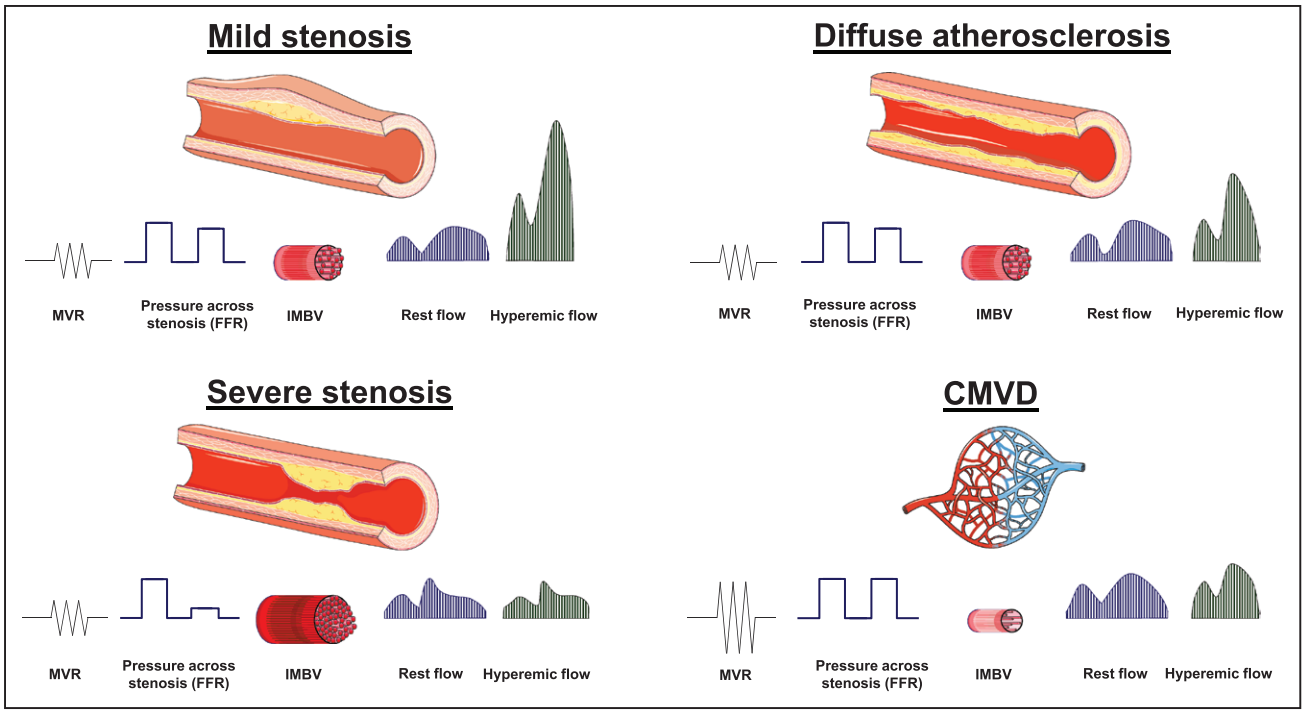

Figure 11. Expected changes in invasive and noninvasive coronary parameters in focal and diffuse atherosclerosis, as well as in coronary microvascular disease (CMVD). In mild nonflow limiting stenosis, microvascular resistance (MVR) is uneffected, and the luminal pressure drop is not sufficient to result in abnormal fractional flow reserve (FFR >0.8). Intramyocardial blood volume (IMBV) would be increased slightly secondary to compensatory vasodilation associated with autoregulation. Coronary flow remains normal under resting conditions and mildly reduced with hyperemic stress. With progression of coronary artery disease (CAD) to severe stenosis, FFR becomes reduced (<0.8), and there is marked increase in IMBV secondary to recruitment and vasodilatation. A severe reduction in baseline flow, hyperemic flow, and CFR can be observed. Diffuse nonobstructive atherosclerotic disease is characterized by gradually decreasing intracoronary pressure across the lesion, mildly increased IMBV and normal resting, and decreased hyperemic myocardial blood flow contributing to reduced CFR. CMVD, on the other hand, is associated with marked increase in coronary vascular resistance, maintained coronary perfusion pressure, and marked reduction in IMBV. Hyperemic myocardial blood flow becomes compromised, leading to reduced CFR.

vasculature. Table 2 summarizes cardiac disorders that have been linked to CMVD.

Reduced hyperemic MBF or reduced CFR has been demonstrated in hypertrophic obstructive cardiomyopathy,[62,103] dilated cardiomyopathy,[107,108] aortic stenosis,[114] amyloidosis,[118] and cardiac allograft vasculopathy.[116] Endothelial dysfunction and CMVD are also recently recognized central components of the pathophysiology of heart failure with preserved ejection fraction.[109,111,112] In many of these myocardial disease states, the impaired coronary flow carries prognostic information,[103,107,117] and improvements in coronary flow parameters have been described after treatment of the underlying cardiac disease.[104,105,113,115] Reduced CFR has been also identified in patients with chronic kidney disease, and CFR has been shown to have a significant positive correlation with GFR in these patients.[119] Additionally, global CFR was shown to be independently associated with all-cause mortality in dialysis-dependent end-stage renal disease patients.[120] Impaired CFR has been also described in a wide variety of chronic autoimmune diseases, including rheumatoid arthritis,[121] systemic lupus erythematosus,[122] and systemic sclerosis.[123] More recently, sarcoid-mediated focal myocardial inflammation has been associated with corresponding regional impairment in coronary flow.[74] In this prospective study, immune suppression

Table 1. Expected Alterations in Invasive and Noninvasive Coronary Flow Indices in CAD and CMVD

	Invasive Indices						
		Noninvasive indices					
Disease	IMR/HMR	FFR/CT-FFR	Rest MBF	Stress MBF	CFR	IMBV	TAG
Mild to moderate nonflow-limiting focal stenosis (<85%)	N	↓	N	↓	↓	↑	↓
Severe, flow-limiting focal stenosis (>85%)	N	↓↓	↓	↓↓	↓↓	↑↑	↓↓
Diffuse atherosclerotic disease	N	↓	N	↓	↓	↑	↓
CMVD	↑↑	N	N/↑	↓	↓	↓↓	N

↓ indicates decrease in index; ↑, increase in index; CAD, coronary artery disease; CFR, coronary flow reserve; CMVD, coronary microvascular disease; FFR, fractional flow reserve; HMR, hyperemic microvascular resistance; IMBV, intramyocardial blood volume; IMR, index of microvascular resistance; MBF, myocardial blood flow; N, no change in index; and TAG, transluminal attenuation gradient. Number of arrows represents the relative magnitude of change.

Table 2. Secondary CMVD in Cardiac Diseases

Disease	Presumed Pathophysiology of CMVD	Coronary Flow Abnormality	Prognostic Value of Coronary Flow Parameters	Improvement in CFR With Treatment	Reference
Hypertrophic obstructive cardiomyopathy	Remodeling of intramural coronary arterioles, marked wall thickening, luminal narrowing	Reduced hyperemic MBF proportional to hypertrophy	Reduced hyperemic MBF independent predictor of cardiovascular death, progression to heart failure, or sustained ventricular arrhythmias	Alcohol septal ablation	Petersen et al[62], Cecchi et al[103], Timmer et al[104]
Dilated cardiomyopathy	Endothelial dysfunction, decreased microvascular density, extravascular compression of the microvasculature because of elevated LV filling pressures	Reduced CFR present at early stage of the disease	Reduced hyperemic MBF independent predictor of cardiac death or development/progression of heart failure Preserved CFR independent predictor of LV recovery in response to CRT	CRT	Djordjevic Dikic et al[105], Knaapen et al[106], Neglia et al[107], van den Heuvel et al[108], Negli et al[124]
Heart failure with preserved ejection fraction	Systemic proinflammatory state leading to coronary microvascular endothelial inflammation, lower coronary microvascular density	Reduced CFR			Kato et al[109], Mohammed et al[110], Paulus and Tschöpe[111], Srivaratharajah et al[112]
Aortic stenosis	Increased hemodynamic load leading to increased LV mass, reduction in diastolic perfusion time, and abnormal cardiac–coronary coupling	Reduced hyperemic flow correlating to stenosis severity		Conventional or transcatheter aortic valve replacement	Rajappan et al[113,114], Wiegerinck et al[115]
Coronary allograft vasculopathy	Generalized endothelial dysfunction, diffuse concentric epicardial intimal thickening with CMVD secondary to changes in sympathetic innervation, inflammation, and autoimmune mechanisms	Reduced CFR correlating with intimal thickening	Reduced CFR and hyperemic MBF predictors of adverse events (all-cause death, acute coronary syndrome, and heart failure hospitalization)		Kofoed et al[116], Mc Ardle et al[117]
Amyloidosis	Diffuse coronary media infiltration or obstruction of intramyocardial coronary vessels by amyloid deposits	Reduced rest MBF, reduced hyperemic MBF, reduced CFR			Dorbala et al[118]
Sarcoidosis	Microvascular compression by inflammation or granulomas	Reduced hyperemic MBF corresponding to areas of inflammation		Immune suppression	Kruse et al[74]

CFR indicates coronary flow reserve; CMVD, coronary microvascular disease; CRT, cardiac resynchronization therapy; LV, left ventricle; and MBF, myocardial blood flow.

induced a decrease in inflammation that was associated with improvement in CFR, whereas CFR further worsened in areas with increasing inflammation.[74]

Conclusions

With the evolution of noninvasive cardiac imaging, absolute quantification of coronary flow became a reality for modern clinical cardiology practice. The evaluation of absolute coronary flow can be used for risk stratification in CAD patients and improves the diagnosis of primary CMVD. Absolute quantification of MBF may also improve our understanding of the pathophysiology behind the cardiac involvement of systemic inflammatory disorders, diseases of the myocardium or vasculature, and the syndrome of heart failure with preserved ejection fraction. In certain diseases, such as diabetes mellitus, hypertrophic obstructive cardiomyopathy, and dilated cardiomyopathy, impaired coronary flow can serve as a powerful prognostic marker, facilitating clinical decision-making regarding clinical surveillance frequency or initiation of more advanced therapies. A progressive decline in coronary physiology can be observed in association with disease progression in certain systemic conditions, such as hypertension, hyperlipidemia, obesity, and diabetes mellitus. Future studies are needed to assess whether noninvasive quantitative assessment of CFR can be applied for monitoring disease progression in these patient populations and to evaluate the clinical impact of early diagnosis and therapy facilitated by noninvasive coronary flow quantification. Future studies are encouraged for the

investigation of whether quantitative assessment of MBF can be used for the prediction of response to therapies, particularly in primary CMVD patients or in patients with heart failure with preserved ejection fraction. The quantification of MBF is expected to become more widely available with advances in technology, and so this invaluable tool can be used in the everyday decision making in clinical cardiology.

Acknowledgments

We thank Dr Zhenwu Zhuang for his help with the acquisition and processing of porcine coronary computed tomography images.

Sources of Funding

This review was supported by a National Institutes of Health (NIH) T32 training grant (HL098069, Sinusas).

Disclosures

None.

References

1. Camici PG, Crea F. Coronary microvascular dysfunction. *N Engl J Med*. 2007;356:830–840. doi: 10.1056/NEJMra061889.
2. Salerno M, Beller GA. Noninvasive assessment of myocardial perfusion. *Circ Cardiovasc Imaging*. 2009;2:412–424. doi: 10.1161/CIRCIMAGING.109.854893.
3. Mekkaoui C, Jadbabaie F, Dione DP, Meoli DF, Purushothaman K, Belardinelli L, Sinusas AJ. Effects of adenosine and a selective A2A adenosine receptor agonist on hemodynamic and thallium-201 and technetium-99m-sestaMIBI biodistribution and kinetics. *JACC Cardiovasc Imaging*. 2009;2:1198–1208. doi: 10.1016/j.jcmg.2009.06.013.
4. Johnson NP, Gould KL. Regadenoson versus dipyridamole hyperemia for cardiac PET imaging. *JACC Cardiovasc Imaging*. 2015;8:438–447. doi: 10.1016/j.jcmg.2014.11.016.
5. Gould KL, Johnson NP, Bateman TM, Beanlands RS, Bengel FM, Bober R, Camici PG, Cerqueira MD, Chow BJ, Di Carli MF, Dorbala S, Gewirtz H, Gropler RJ, Kaufmann PA, Knaapen P, Knuuti J, Merhige ME, Rentrop KP, Ruddy TD, Schelbert HR, Schindler TH, Schwaiger M, Sdringola S, Vitarello J, Williams KA Sr, Gordon D, Dilsizian V, Narula J. Anatomic versus physiologic assessment of coronary artery disease. Role of coronary flow reserve, fractional flow reserve, and positron emission tomography imaging in revascularization decision-making. *J Am Coll Cardiol*. 2013;62:1639–1653. doi: 10.1016/j.jacc.2013.07.076.
6. Morita K, Tsukamoto T, Naya M, Noriyasu K, Inubushi M, Shiga T, Katoh C, Kuge Y, Tsutsui H, Tamaki N. Smoking cessation normalizes coronary endothelial vasomotor response assessed with 15O-water and PET in healthy young smokers. *J Nucl Med*. 2006;47:1914–1920.
7. Schindler TH, Cardenas J, Prior JO, Facta AD, Kreissl MC, Zhang XL, Sayre J, Dahlbom M, Licinio J, Schelbert HR. Relationship between increasing body weight, insulin resistance, inflammation, adipocytokine leptin, and coronary circulatory function. *J Am Coll Cardiol*. 2006;47:1188–1195. doi: 10.1016/j.jacc.2005.10.062.
8. Quercioli A, Montecucco F, Pataky Z, Thomas A, Ambrosio G, Staub C, Di Marzo V, Ratib O, Mach F, Golay A, Schindler TH. Improvement in coronary circulatory function in morbidly obese individuals after gastric bypass-induced weight loss: relation to alterations in endocannabinoids and adipocytokines. *Eur Heart J*. 2013;34:2063–2073. doi: 10.1093/eurheartj/eht085.
9. Alexánderson E, Ochoa JM, Calleja R, Juárez-Rojas JG, Prior JO, Jácome R, Romero E, Meave A, Posadas-Romero C. Endothelial dysfunction in systemic lupus erythematosus: evaluation with 13N-ammonia PET. *J Nucl Med*. 2010;51:1927–1931. doi: 10.2967/jnumed.110.078212.
10. Prior JO, Quiñones MJ, Hernandez-Pampaloni M, Facta AD, Schindler TH, Sayre JW, Hsueh WA, Schelbert HR. Coronary circulatory dysfunction in insulin resistance, impaired glucose tolerance, and type 2 diabetes mellitus. *Circulation*. 2005;111:2291–2298. doi: 10.1161/01.CIR.0000164232.62768.51.
11. Jayaweera AR, Edwards N, Glasheen WP, Villanueva FS, Abbott RD, Kaul S. *In vivo* myocardial kinetics of air-filled albumin microbubbles during myocardial contrast echocardiography. Comparison with radiolabeled red blood cells. *Circ Res*. 1994;74:1157–1165.
12. Wei K, Jayaweera AR, Firoozan S, Linka A, Skyba DM, Kaul S. Quantification of myocardial blood flow with ultrasound-induced destruction of microbubbles administered as a constant venous infusion. *Circulation*. 1998;97:473–483.
13. Wu CC, Feldman MD, Mills JD, Manaugh CA, Fischer D, Jafar MZ, Villanueva FS. Myocardial contrast echocardiography can be used to quantify intramyocardial blood volume: new insights into structural mechanisms of coronary autoregulation. *Circulation*. 1997;96:1004–1011.
14. McCommis KS, Zhang H, Goldstein TA, Misselwitz B, Abendschein DR, Gropler RJ, Zheng J. Myocardial blood volume is associated with myocardial oxygen consumption: an experimental study with cardiac magnetic resonance in a canine model. *JACC Cardiovasc Imaging*. 2009;2:1313–1320. doi: 10.1016/j.jcmg.2009.07.010.
15. Möhlenkamp S, Beighley PE, Pfeifer EA, Behrenbeck TR, Sheedy PF 2nd, Ritman EL. Intramyocardial blood volume, perfusion and transit time in response to embolization of different sized microvessels. *Cardiovasc Res*. 2003;57:843–852.
16. Lindner JR, Skyba DM, Goodman NC, Jayaweera AR, Kaul S. Changes in myocardial blood volume with graded coronary stenosis. *Am J Physiol*. 1997;272(1 pt 2):H567–H575.
17. Indermühle A, Vogel R, Meier P, Wirth S, Stoop R, Mohaupt MG, Seiler C. The relative myocardial blood volume differentiates between hypertensive heart disease and athlete's heart in humans. *Eur Heart J*. 2006;27:1571–1578. doi: 10.1093/eurheartj/ehl024.
18. Choi JH, Min JK, Labounty TM, Lin FY, Mendoza DD, Shin DH, Ariaratnam NS, Koduru S, Granada JF, Gerber TC, Oh JK, Gwon HC, Choe YH. Intracoronary transluminal attenuation gradient in coronary CT angiography for determining coronary artery stenosis. *JACC Cardiovasc Imaging*. 2011;4:1149–1157. doi: 10.1016/j.jcmg.2011.09.006.
19. Koo BK, Erglis A, Doh JH, Daniels DV, Jegere S, Kim HS, Dunning A, DeFrance T, Lansky A, Leipsic J, Min JK. Diagnosis of ischemia-causing coronary stenoses by noninvasive fractional flow reserve computed from coronary computed tomographic angiograms. Results from the prospective multicenter DISCOVER-FLOW (Diagnosis of Ischemia-Causing Stenoses Obtained Via Noninvasive Fractional Flow Reserve) study. *J Am Coll Cardiol*. 2011;58:1989–1997. doi: 10.1016/j.jacc.2011.06.066.
20. Bergmann SR, Herrero P, Markham J, Weinheimer CJ, Walsh MN. Noninvasive quantitation of myocardial blood flow in human subjects with oxygen-15-labeled water and positron emission tomography. *J Am Coll Cardiol*. 1989;14:639–652.
21. Geltman EM, Henes CG, Senneff MJ, Sobel BE, Bergmann SR. Increased myocardial perfusion at rest and diminished perfusion reserve in patients with angina and angiographically normal coronary arteries. *J Am Coll Cardiol*. 1990;16:586–595.
22. Sara JD, Widmer RJ, Matsuzawa Y, Lennon RJ, Lerman LO, Lerman A. Prevalence of coronary microvascular dysfunction among patients with chest pain and nonobstructive coronary artery disease. *JACC Cardiovasc Interv*. 2015;8:1445–1453. doi: 10.1016/j.jcin.2015.06.017.
23. Gullberg GT, Reutter BW, Sitek A, Maltz JS, Budinger TF. Dynamic single photon emission computed tomography–basic principles and cardiac applications. *Phys Med Biol*. 2010;55:R111–R191. doi: 10.1088/0031-9155/55/20/R01.
24. Bergmann SR, Fox KA, Rand AL, McElvany KD, Welch MJ, Markham J, Sobel BE. Quantification of regional myocardial blood flow *in vivo* with H215O. *Circulation*. 1984;70:724–733.
25. Bol A, Melin JA, Vanoverschelde JL, Baudhuin T, Vogelaers D, De Pauw M, Michel C, Luxen A, Labar D, Cogneau M. Direct comparison of [13N]ammonia and [15O]water estimates of perfusion with quantification of regional myocardial blood flow by microspheres. *Circulation*. 1993;87:512–525.
26. Kuhle WG, Porenta G, Huang SC, Buxton D, Gambhir SS, Hansen H, Phelps ME, Schelbert HR. Quantification of regional myocardial blood flow using 13N-ammonia and reoriented dynamic positron emission tomographic imaging. *Circulation*. 1992;86:1004–1017.
27. Mullani NA, Goldstein RA, Gould KL, Marani SK, Fisher DJ, O'Brien HA Jr, Loberg MD. Myocardial perfusion with rubidium-82. I. Measurement of extraction fraction and flow with external detectors. *J Nucl Med*. 1983;24:898–906.
28. El Fakhri G, Kardan A, Sitek A, Dorbala S, Abi-Hatem N, Lahoud Y, Fischman A, Coughlan M, Yasuda T, Di Carli MF. Reproducibility and accuracy of quantitative myocardial blood flow assessment with (82)Rb PET: comparison with (13)N-ammonia PET. *J Nucl Med*. 2009;50:1062–1071. doi: 10.2967/jnumed.104.007831.

29. Huisman MC, Higuchi T, Reder S, Nekolla SG, Poethko T, Wester HJ, Ziegler SI, Casebier DS, Robinson SP, Schwaiger M. Initial characterization of an 18F-labeled myocardial perfusion tracer. *J Nucl Med*. 2008;49:630–636. doi: 10.2967/jnumed.107.044727.
30. Nekolla SG, Reder S, Saraste A, Higuchi T, Dzewas G, Preissel A, Huisman M, Poethko T, Schuster T, Yu M, Robinson S, Casebier D, Henke J, Wester HJ, Schwaiger M. Evaluation of the novel myocardial perfusion positron-emission tomography tracer 18F-BMS-747158-02: comparison to 13N-ammonia and validation with microspheres in a pig model. *Circulation*. 2009;119:2333–2342. doi: 10.1161/CIRCULATIONAHA.108.797761.
31. Berman DS, Maddahi J, Tamarappoo BK, Czernin J, Taillefer R, Udelson JE, Gibson CM, Devine M, Lazewatsky J, Bhat G, Washburn D. Phase II safety and clinical comparison with single-photon emission computed tomography myocardial perfusion imaging for detection of coronary artery disease: flurpiridaz F 18 positron emission tomography. *J Am Coll Cardiol*. 2013;61:469–477. doi: 10.1016/j.jacc.2012.11.022.
32. Maddahi J and Packard RR. PET should replace SPECT in cardiac imaging for diagnosis and risk assessment of patients with known or suspected CAD: Pro. *J Nucl Cardiol*. 2017. In press.
33. Lautamäki R, George RT, Kitagawa K, Higuchi T, Merrill J, Voicu C, DiPaula A, Nekolla SG, Lima JA, Lardo AC, Bengel FM. Rubidium-82 PET-CT for quantitative assessment of myocardial blood flow: validation in a canine model of coronary artery stenosis. *Eur J Nucl Med Mol Imaging*. 2009;36:576–586. doi: 10.1007/s00259-008-0972-1.
34. Nesterov SV, Deshayes E, Sciagrà R, Settimo L, Declerck JM, Pan XB, Yoshinaga K, Katoh C, Slomka PJ, Germano G, Han C, Aalto V, Alessio AM, Ficaro EP, Lee BC, Nekolla SG, Gwet KL, deKemp RA, Klein R, Dickson J, Case JA, Bateman T, Prior JO, Knuuti JM. Quantification of myocardial blood flow in absolute terms using (82)Rb PET imaging: the RUBY-10 Study. *JACC Cardiovasc Imaging*. 2014;7:1119–1127. doi: 10.1016/j.jcmg.2014.08.003.
35. Hsu B, Hu LH, Yang BH, Chen LC, Chen YK, Ting CH, Hung GU, Huang WS, Wu TC. SPECT myocardial blood flow quantitation toward clinical use: a comparative study with (13)N-Ammonia PET myocardial blood flow quantitation. *Eur J Nucl Med Mol Imaging*. 2017;44:117–128. doi: 10.1007/s00259-016-3491-5.
36. Nkoulou R, Fuchs TA, Pazhenkottil AP, Kuest SM, Ghadri JR, Stehli J, Fiechter M, Herzog BA, Gaemperli O, Buechel RR, Kaufmann PA. Absolute myocardial blood flow and flow reserve assessed by gated SPECT with cadmium-zinc-telluride detectors using 99mTc-tetrofosmin: head-to-head comparison with 13N-ammonia PET. *J Nucl Med*. 2016;57:1887–1892. doi: 10.2967/jnumed.115.165498.
37. Wells RG, Timmins R, Klein R, Lockwood J, Marvin B, deKemp RA, Wei L, Ruddy TD. Dynamic SPECT measurement of absolute myocardial blood flow in a porcine model. *J Nucl Med*. 2014;55:1685–1691. doi: 10.2967/jnumed.114.139782.
38. Rumsey WL, Rosenspire KC, Nunn AD. Myocardial extraction of teboroxime: effects of teboroxime interaction with blood. *J Nucl Med*. 1992;33:94–101.
39. Iida H, Eberl S. Quantitative assessment of regional myocardial blood flow with thallium-201 and SPECT. *J Nucl Cardiol*. 1998;5:313–331.
40. Weich HF, Strauss HW, Pitt B. The extraction of thallium-201 by the myocardium. *Circulation*. 1977;56:188–191.
41. Broisat A, Ruiz M, Goodman NC, Hanrahan SM, Reutter BW, Brennan KM, Janabi M, Schaefer S, Watson DD, Beller GA, VanBrocklin HF, Glover DK. Myocardial uptake of 7'-(Z)-[(123)I] iodorotenone during vasodilator stress in dogs with critical coronary stenoses. *Circ Cardiovasc Imaging*. 2011;4:685–692. doi: 10.1161/CIRCIMAGING.110.961763.
42. Wells RG, Wei L, Petryk J, Duan Y, Marvin B, Timmins R, Soueidan K, Fernando P, Bensimon C, Ruddy TD. Flow-dependent uptake of ^{123}I-CMICE-013, a novel SPECT perfusion agent, compared with standard tracers. *J Nucl Med*. 2015;56:764–770. doi: 10.2967/jnumed.114.151563.
43. Liu C, Sinusas AJ. Is assessment of absolute myocardial perfusion with SPECT ready for prime time? *J Nucl Med*. 2014;55:1573–1575. doi: 10.2967/jnumed.114.144550.
44. Tatineni S, Kern MJ, Deligonul U, Aguirre F. The effects of ionic and nonionic radiographic contrast media on coronary hyperemia in patients during coronary angiography. *Am Heart J*. 1992;123:621–627.
45. Canty JM Jr, Judd RM, Brody AS, Klocke FJ. First-pass entry of nonionic contrast agent into the myocardial extravascular space. Effects on radiographic estimates of transit time and blood volume. *Circulation*. 1991;84:2071–2078.
46. Kühl JT, George RT, Mehra VC, Linde JJ, Chen M, Arai AE, Di Carli M, Kitagawa K, Dewey M, Lima JA, Kofoed KF. Endocardial-epicardial distribution of myocardial perfusion reserve assessed by multidetector computed tomography in symptomatic patients without significant coronary artery disease: insights from the CORE320 multicentre study. *Eur Heart J Cardiovasc Imaging*. 2016;17:779–787. doi: 10.1093/ehjci/jev206.
47. Nakazato R, Park HB, Berman DS, Gransar H, Koo BK, Erglis A, Lin FY, Dunning AM, Budoff MJ, Malpeso J, Leipsic J, Min JK. Noninvasive fractional flow reserve derived from computed tomography angiography for coronary lesions of intermediate stenosis severity: results from the DeFACTO study. *Circ Cardiovasc Imaging*. 2013;6:881–889. doi: 10.1161/CIRCIMAGING.113.000297.
48. Danad I, Raijmakers PG, Appelman YE, Harms HJ, de Haan S, van den Oever ML, Heymans MW, Tulevski II, van Kuijk C, Hoekstra OS, Lammertsma AA, Lubberink M, van Rossum AC, Knaapen P. Hybrid imaging using quantitative H215O PET and CT-based coronary angiography for the detection of coronary artery disease. *J Nucl Med*. 2013;54:55–63. doi: 10.2967/jnumed.112.104687.
49. So A, Hsieh J, Li JY, Hadway J, Kong HF, Lee TY. Quantitative myocardial perfusion measurement using CT perfusion: a validation study in a porcine model of reperfused acute myocardial infarction. *Int J Cardiovasc Imaging*. 2012;28:1237–1248. doi: 10.1007/s10554-011-9927-x.
50. So A, Hsieh J, Imai Y, Narayanan S, Kramer J, Procknow K, Dutta S, Leipsic J, Min JK, Labounty T, Lee TY. Prospectively ECG-triggered rapid kV-switching dual-energy CT for quantitative imaging of myocardial perfusion. *JACC Cardiovasc Imaging*. 2012;5:829–836. doi: 10.1016/j.jcmg.2011.12.026.
51. Vliegenthart R, De Cecco CN, Wichmann JL, Meinel FG, Pelgrim GJ, Tesche C, Ebersberger U, Pugliese F, Bamberg F, Choe YH, Wang Y, Schoepf UJ. Dynamic CT myocardial perfusion imaging identifies early perfusion abnormalities in diabetes and hypertension: Insights from a multicenter registry. *J Cardiovasc Comput Tomogr*. 2016;10:301–308. doi: 10.1016/j.jcct.2016.05.005.
52. Ishida M, Ichihara T, Nagata M, Ishida N, Takase S, Kurita T, Ito M, Takeda K, Sakuma H. Quantification of myocardial blood flow using model based analysis of first-pass perfusion MRI: extraction fraction of Gd-DTPA varies with myocardial blood flow in human myocardium. *Magn Reson Med*. 2011;66:1391–1399. doi: 10.1002/mrm.22936.
53. Ishida M, Schuster A, Morton G, Chiribiri A, Hussain S, Paul M, Merkle N, Steen H, Lossnitzer D, Schnackenburg B, Alfakih K, Plein S, Nagel E. Development of a universal dual-bolus injection scheme for the quantitative assessment of myocardial perfusion cardiovascular magnetic resonance. *J Cardiovasc Magn Reson*. 2011;13:28. doi: 10.1186/1532-429X-13-28.
54. Patel AR, Antkowiak PF, Nandalur KR, West AM, Salerno M, Arora V, Christopher J, Epstein FH, Kramer CM. Assessment of advanced coronary artery disease: advantages of quantitative cardiac magnetic resonance perfusion analysis. *J Am Coll Cardiol*. 2010;56:561–569. doi: 10.1016/j.jacc.2010.02.061.
55. Ichihara T, Ishida M, Kitagawa K, Ichikawa Y, Natsume T, Yamaki N, Maeda H, Takeda K, Sakuma H. Quantitative analysis of first-pass contrast-enhanced myocardial perfusion MRI using a Patlak plot method and blood saturation correction. *Magn Reson Med*. 2009;62:373–383. doi: 10.1002/mrm.22018.
56. Schuster A, Zarinabad N, Ishida M, Sinclair M, van den Wijngaard JP, Morton G, Hautvast GL, Bigalke B, van Horssen P, Smith N, Spaan JA, Siebes M, Chiribiri A, Nagel E. Quantitative assessment of magnetic resonance derived myocardial perfusion measurements using advanced techniques: microsphere validation in an explanted pig heart system. *J Cardiovasc Magn Reson*. 2014;16:82. doi: 10.1186/s12968-014-0082-0.
57. Christian TF, Rettmann DW, Aletras AH, Liao SL, Taylor JL, Balaban RS, Arai AE. Absolute myocardial perfusion in canines measured by using dual-bolus first-pass MR imaging. *Radiology*. 2004;232:677–684. doi: 10.1148/radiol.2323030573.
58. Jerosch-Herold M, Swingen C, Seethamraju RT. Myocardial blood flow quantification with MRI by model-independent deconvolution. *Med Phys*. 2002;29:886–897. doi: 10.1118/1.1473135.
59. Biglands JD, Magee DR, Sourbron SP, Plein S, Greenwood JP, Radjenovic A. Comparison of the diagnostic performance of four quantitative myocardial perfusion estimation methods used in cardiac MR imaging: CE-MARC Substudy. *Radiology*. 2015;275:393–402. doi: 10.1148/radiol.14140433.
60. Di Bella EV, Parker DL, Sinusas AJ. On the dark rim artifact in dynamic contrast-enhanced MRI myocardial perfusion studies. *Magn Reson Med*. 2005;54:1295–1299. doi: 10.1002/mrm.20666.

61. Liu A, Wijesurendra RS, Francis JM, Robson MD, Neubauer S, Piechnik SK, Ferreira VM. Adenosine stress and rest T1 mapping can differentiate between ischemic, infarcted, remote, and normal myocardium without the need for gadolinium contrast agents. *JACC Cardiovasc Imaging*. 2016;9:27–36. doi: 10.1016/j.jcmg.2015.08.018.
62. Petersen SE, Jerosch-Herold M, Hudsmith LE, Robson MD, Francis JM, Doll HA, Selvanayagam JB, Neubauer S, Watkins H. Evidence for microvascular dysfunction in hypertrophic cardiomyopathy: new insights from multiparametric magnetic resonance imaging. *Circulation*. 2007;115:2418–2425. doi: 10.1161/CIRCULATIONAHA.106.657023.
63. Vogel R, Indermühle A, Reinhardt J, Meier P, Siegrist PT, Namdar M, Kaufmann PA, Seiler C. The quantification of absolute myocardial perfusion in humans by contrast echocardiography: algorithm and validation. *J Am Coll Cardiol*. 2005;45:754–762. doi: 10.1016/j.jacc.2004.11.044.
64. Pascotto M, Wei K, Micari A, Bragadeesh T, Goodman NC, Kaul S. Phasic changes in arterial blood volume is influenced by collateral blood flow: implications for the quantification of coronary stenosis at rest. *Heart*. 2007;93:438–443. doi: 10.1136/hrt.2006.089631.
65. Wei K, Le E, Jayaweera AR, Bin JP, Goodman NC, Kaul S. Detection of noncritical coronary stenosis at rest without recourse to exercise or pharmacological stress. *Circulation*. 2002;105:218–223.
66. Le DE, Bragadeesh T, Zhao Y, Wang YG, Zha D, Kaul S. Detection of coronary stenosis with myocardial contrast echocardiography using regadenoson, a selective adenosine A2A receptor agonist. *Eur Heart J Cardiovasc Imaging*. 2012;13:298–308. doi: 10.1093/ejechocard/jer232.
67. Feher A, Chen SY, Bagi Z, Arora V. Prevention and treatment of no-reflow phenomenon by targeting the coronary microcirculation. *Rev Cardiovasc Med*. 2014;15:38–51.
68. Sinusas AJ, Bengel F, Nahrendorf M, Epstein FH, Wu JC, Villanueva FS, Fayad ZA, Gropler RJ. Multimodality cardiovascular molecular imaging, part I. *Circ Cardiovasc Imaging*. 2008;1:244–256. doi: 10.1161/CIRCIMAGING.108.824359.
69. Di Carli MF, Bianco-Batlles D, Landa ME, Kazmers A, Groehn H, Muzik O, Grunberger G. Effects of autonomic neuropathy on coronary blood flow in patients with diabetes mellitus. *Circulation*. 1999;100:813–819.
70. Lanza GA, Giordano A, Pristipino C, Calcagni ML, Meduri G, Trani C, Franceschini R, Crea F, Troncone L, Maseri A. Abnormal cardiac adrenergic nerve function in patients with syndrome X detected by [123I]metaiodobenzylguanidine myocardial scintigraphy. *Circulation*. 1997;96:821–826.
71. Di Carli MF, Tobes MC, Mangner T, Levine AB, Muzik O, Chakroborty P, Levine TB. Effects of cardiac sympathetic innervation on coronary blood flow. *N Engl J Med*. 1997;336:1208–1215. doi: 10.1056/NEJM199704243361703.
72. Sun KT, Yeatman LA, Buxton DB, Chen K, Johnson JA, Huang SC, Kofoed KF, Weismueller S, Czernin J, Phelps ME, Schelbert HR. Simultaneous measurement of myocardial oxygen consumption and blood flow using [1-carbon-11]acetate. *J Nucl Med*. 1998;39:272–280.
73. Tillisch J, Brunken R, Marshall R, Schwaiger M, Mandelkern M, Phelps M, Schelbert H. Reversibility of cardiac wall-motion abnormalities predicted by positron tomography. *N Engl J Med*. 1986;314:884–888. doi: 10.1056/NEJM198604033141405.
74. Kruse MJ, Kovell L, Kasper EK, Pomper MG, Moller DR, Solnes L, Chen ES, Schindler TH. Myocardial blood flow and inflammatory cardiac sarcoidosis. *JACC Cardiovasc Imaging*. 2017;10:157–167. doi: 10.1016/j.jcmg.2016.09.023.
75. Bøttcher M, Botker HE, Sonne H, Nielsen TT, Czernin J. Endothelium-dependent and -independent perfusion reserve and the effect of L-arginine on myocardial perfusion in patients with syndrome X. *Circulation*. 1999;99:1795–1801.
76. Recio-Mayoral A, Rimoldi OE, Camici PG, Kaski JC. Inflammation and microvascular dysfunction in cardiac syndrome X patients without conventional risk factors for coronary artery disease. *JACC Cardiovasc Imaging*. 2013;6:660–667. doi: 10.1016/j.jcmg.2012.12.011.
77. Reis SE, Holubkov R, Conrad Smith AJ, Kelsey SF, Sharaf BL, Reichek N, Rogers WJ, Merz CN, Sopko G, Pepine CJ; WISE Investigators. Coronary microvascular dysfunction is highly prevalent in women with chest pain in the absence of coronary artery disease: results from the NHLBI WISE study. *Am Heart J*. 2001;141:735–741.
78. Crea F, Camici PG, Bairey Merz CN. Coronary microvascular dysfunction: an update. *Eur Heart J*. 2014;35:1101–1111. doi: 10.1093/eurheartj/eht513.
79. Gulati M, Cooper-DeHoff RM, McClure C, Johnson BD, Shaw LJ, Handberg EM, Zineh I, Kelsey SF, Arnsdorf MF, Black HR, Pepine CJ, Merz CN. Adverse cardiovascular outcomes in women with nonobstructive coronary artery disease: a report from the Women's Ischemia Syndrome Evaluation Study and the St James Women Take Heart Project. *Arch Intern Med*. 2009;169:843–850. doi: 10.1001/archinternmed.2009.50.
80. Pepine CJ, Anderson RD, Sharaf BL, Reis SE, Smith KM, Handberg EM, Johnson BD, Sopko G, Bairey Merz CN. Coronary microvascular reactivity to adenosine predicts adverse outcome in women evaluated for suspected ischemia results from the National Heart, Lung and Blood Institute WISE (Women's Ischemia Syndrome Evaluation) study. *J Am Coll Cardiol*. 2010;55:2825–2832. doi: 10.1016/j.jacc.2010.01.054.
81. Amsterdam EA, Wenger NK, Brindis RG, Casey DE Jr, Ganiats TG, Holmes DR Jr, Jaffe AS, Jneid H, Kelly RF, Kontos MC, Levine GN, Liebson PR, Mukherjee D, Peterson ED, Sabatine MS, Smalling RW, Zieman SJ; ACC/AHA Task Force Members. 2014 AHA/ACC guideline for the management of patients with non-ST-elevation acute coronary syndromes: a report of the American College of Cardiology/American Heart Association Task Force on Practice Guidelines. *Circulation*. 2014;130:e344–e426. doi: 10.1161/CIR.0000000000000134.
82. Montalescot G, Sechtem U, Achenbach S, Andreotti F, Arden C, Budaj A, Bugiardini R, Crea F, Cuisset T, Di Mario C, Ferreira JR, Gersh BJ, Gitt AK, Hulot JS, Marx N, Opie LH, Pfisterer M, Prescott E, Ruschitzka F, Sabaté M, Senior R, Taggart DP, van der Wall EE, Vrints CJ, Zamorano JL, Achenbach S, Baumgartner H, Bax JJ, Bueno H, Dean V, Deaton C, Erol C, Fagard R, Ferrari R, Hasdai D, Hoes AW, Kirchhof P, Knuuti J, Kolh P, Lancellotti P, Linhart A, Nihoyannopoulos P, Piepoli MF, Ponikowski P, Sirnes PA, Tamargo JL, Tendera M, Torbicki A, Wijns W, Windecker S, Knuuti J, Valgimigli M, Bueno H, Claeys MJ, Donner-Banzhoff N, Erol C, Frank H, Funck-Brentano C, Gaemperli O, Gonzalez-Juanatey JR, Hamilos M, Hasdai D, Husted S, James SK, Kervinen K, Kolh P, Kristensen SD, Lancellotti P, Maggioni AP, Piepoli MF, Pries AR, Romeo F, Rydén L, Simoons ML, Sirnes PA, Steg PG, Timmis A, Wijns W, Windecker S, Yildirir A, Zamorano JL; Task Force Members; ESC Committee for Practice Guidelines; Document Reviewers. 2013 ESC guidelines on the management of stable coronary artery disease: the Task Force on the management of stable coronary artery disease of the European Society of Cardiology. *Eur Heart J*. 2013;34:2949–3003. doi: 10.1093/eurheartj/eht296.
83. Safdar B, D'Onofrio G, Dziura J, Russell RR, Johnson C, Sinusas AJ. Ranolazine and microvascular angina by PET in the emergency department: results from a pilot randomized controlled trial. *Clin Ther*. 2017;39:55–63. doi: 10.1016/j.clinthera.2016.12.002.
84. Czernin J, Müller P, Chan S, Brunken RC, Porenta G, Krivokapich J, Chen K, Chan A, Phelps ME, Schelbert HR. Influence of age and hemodynamics on myocardial blood flow and flow reserve. *Circulation*. 1993;88:62–69.
85. Uren NG, Camici PG, Melin JA, Bol A, de Bruyne B, Radvan J, Olivotto I, Rosen SD, Impallomeni M, Wijns W. Effect of aging on myocardial perfusion reserve. *J Nucl Med*. 1995;36:2032–2036.
86. Kaufmann PA, Gnecchi-Ruscone T, di Terlizzi M, Schäfers KP, Lüscher TF, Camici PG. Coronary heart disease in smokers: vitamin C restores coronary microcirculatory function. *Circulation*. 2000;102:1233–1238.
87. Rimoldi O, Rosen SD, Camici PG. The blunting of coronary flow reserve in hypertension with left ventricular hypertrophy is transmural and correlates with systolic blood pressure. *J Hypertens*. 2014;32:2465–2471; discussion 2471. doi: 10.1097/HJH.0000000000000338.
88. Erdogan D, Yildirim I, Ciftci O, Ozer I, Caliskan M, Gullu H, Muderrisoglu H. Effects of normal blood pressure, prehypertension, and hypertension on coronary microvascular function. *Circulation*. 2007;115:593–599. doi: 10.1161/CIRCULATIONAHA.106.650747.
89. Neglia D, Fommei E, Varela-Carver A, Mancini M, Ghione S, Lombardi M, Pisani P, Parker H, D'amati G, Donato L, Camici PG. Perindopril and indapamide reverse coronary microvascular remodelling and improve flow in arterial hypertension. *J Hypertens*. 2011;29:364–372. doi: 10.1097/HJH.0b013e328340a08e.
90. Yokoyama I, Ohtake T, Momomura S, Nishikawa J, Sasaki Y, Omata M. Reduced coronary flow reserve in hypercholesterolemic patients without overt coronary stenosis. *Circulation*. 1996;94:3232–3238.
91. Guethlin M, Kasel AM, Coppenrath K, Ziegler S, Delius W, Schwaiger M. Delayed response of myocardial flow reserve to lipid-lowering therapy with fluvastatin. *Circulation*. 1999;99:475–481.
92. Naoumova RP, Kindler H, Leccisotti L, Mongillo M, Khan MT, Neuwirth C, Seed M, Holvoet P, Betteridge J, Camici PG. Pioglitazone improves myocardial blood flow and glucose utilization in nondiabetic patients with combined hyperlipidemia: a randomized, double-blind,

placebo-controlled study. *J Am Coll Cardiol*. 2007;50:2051–2058. doi: 10.1016/j.jacc.2007.07.070.
93. Murthy VL, Naya M, Foster CR, Gaber M, Hainer J, Klein J, Dorbala S, Blankstein R, Di Carli MF. Association between coronary vascular dysfunction and cardiac mortality in patients with and without diabetes mellitus. *Circulation*. 2012;126:1858–1868. doi: 10.1161/CIRCULATIONAHA.112.120402.
94. Dandekar VK, Bauml MA, Ertel AW, Dickens C, Gonzalez RC, Farzaneh-Far A. Assessment of global myocardial perfusion reserve using cardiovascular magnetic resonance of coronary sinus flow at 3 Tesla. *J Cardiovasc Magn Reson*. 2014;16:24. doi: 10.1186/1532-429X-16-24.
95. Sambuceti G, Marzullo P, Giorgetti A, Neglia D, Marzilli M, Salvadori P, L'Abbate A, Parodi O. Global alteration in perfusion response to increasing oxygen consumption in patients with single-vessel coronary artery disease. *Circulation*. 1994;90:1696–1705.
96. Liga R, Marini C, Coceani M, Filidei E, Schlueter M, Bianchi M, Rossi G, Pardini S, Salvadori P, Parodi O, Rovai D, Sambuceti G, Marraccini P, Neglia D. Structural abnormalities of the coronary arterial wall–in addition to luminal narrowing–affect myocardial blood flow reserve. *J Nucl Med*. 2011;52:1704–1712. doi: 10.2967/jnumed.111.091009.
97. Murthy VL, Naya M, Foster CR, Hainer J, Gaber M, Di Carli G, Blankstein R, Dorbala S, Sitek A, Pencina MJ, Di Carli MF. Improved cardiac risk assessment with noninvasive measures of coronary flow reserve. *Circulation*. 2011;124:2215–2224. doi: 10.1161/CIRCULATIONAHA.111.050427.
98. De Bruyne B, Pijls NH, Kalesan B, Barbato E, Tonino PA, Piroth Z, Jagic N, Möbius-Winkler S, Mobius-Winckler S, Rioufol G, Witt N, Kala P, MacCarthy P, Engström T, Oldroyd KG, Mavromatis K, Manoharan G, Verlee P, Frobert O, Curzen N, Johnson JB, Jüni P, Fearon WF; FAME 2 Trial Investigators. Fractional flow reserve-guided PCI versus medical therapy in stable coronary disease. *N Engl J Med*. 2012;367:991–1001. doi: 10.1056/NEJMoa1205361.
99. van de Hoef TP, van Lavieren MA, Damman P, Delewi R, Piek MA, Chamuleau SA, Voskuil M, Henriques JP, Koch KT, de Winter RJ, Spaan JA, Siebes M, Tijssen JG, Meuwissen M, Piek JJ. Physiological basis and long-term clinical outcome of discordance between fractional flow reserve and coronary flow velocity reserve in coronary stenoses of intermediate severity. *Circ Cardiovasc Interv*. 2014;7:301–311. doi: 10.1161/CIRCINTERVENTIONS.113.001049.
100. De Bruyne B, Hersbach F, Pijls NH, Bartunek J, Bech JW, Heyndrickx GR, Gould KL, Wijns W. Abnormal epicardial coronary resistance in patients with diffuse atherosclerosis but "Normal" coronary angiography. *Circulation*. 2001;104:2401–2406.
101. Maes A, Van de Werf F, Nuyts J, Bormans G, Desmet W, Mortelmans L. Impaired myocardial tissue perfusion early after successful thrombolysis. Impact on myocardial flow, metabolism, and function at late follow-up. *Circulation*. 1995;92:2072–2078.
102. Teunissen PF, de Waard GA, Hollander MR, Robbers LF, Danad I, Biesbroek PS, Amier RP, Echavarría-Pinto M, Quirós A, Broyd C, Heymans MW, Nijveldt R, Lammertsma AA, Raijmakers PG, Allaart CP, Lemkes JS, Appelman YE, Marques KM, Bronzwaer JG, Horrevoets AJ, van Rossum AC, Escaned J, Beek AM, Knaapen P, van Royen N. Doppler-derived intracoronary physiology indices predict the occurrence of microvascular injury and microvascular perfusion deficits after angiographically successful primary percutaneous coronary intervention. *Circ Cardiovasc Interv*. 2015;8:e001786. doi: 10.1161/CIRCINTERVENTIONS.114.001786.
103. Cecchi F, Olivotto I, Gistri R, Lorenzoni R, Chiriatti G, Camici PG. Coronary microvascular dysfunction and prognosis in hypertrophic cardiomyopathy. *N Engl J Med*. 2003;349:1027–1035. doi: 10.1056/NEJMoa025050.
104. Timmer SA, Knaapen P, Germans T, Dijkmans PA, Lubberink M, Ten Berg JM, Ten Cate FJ, Rüssel IK, Götte MJ, Lammertsma AA, van Rossum AC. Effects of alcohol septal ablation on coronary microvascular function and myocardial energetics in hypertrophic obstructive cardiomyopathy. *Am J Physiol Heart Circ Physiol*. 2011;301:H129–H137. doi: 10.1152/ajpheart.00077.2011.
105. Djordjevic Dikic A, Nikcevic G, Raspopovic S, Jovanovic V, Tesic M, Beleslin B, Stepanovic J, Giga V, Milasinovic G. Prognostic role of coronary flow reserve for left ventricular functional improvement after cardiac resynchronization therapy in patients with dilated cardiomyopathy. *Eur Heart J Cardiovasc Imaging*. 2014;15:1344–1349. doi: 10.1093/ehjci/jeu136.
106. Knaapen P, van Campen LM, de Cock CC, Götte MJ, Visser CA, Lammertsma AA, Visser FC. Effects of cardiac resynchronization therapy on myocardial perfusion reserve. *Circulation*. 2004;110:646–651. doi: 10.1161/01.CIR.0000138108687.19.C1.
107. Neglia D, Parodi O, Gallopin M, Sambuceti G, Giorgetti A, Pratali L, Salvadori P, Michelassi C, Lunardi M, Pelosi G. Myocardial blood flow response to pacing tachycardia and to dipyridamole infusion in patients with dilated cardiomyopathy without overt heart failure. A quantitative assessment by positron emission tomography. *Circulation*. 1995;92:796–804.
108. van den Heuvel AF, van Veldhuisen DJ, van der Wall EE, Blanksma PK, Siebelink HM, Vaalburg WM, van Gilst WH, Crijns HJ. Regional myocardial blood flow reserve impairment and metabolic changes suggesting myocardial ischemia in patients with idiopathic dilated cardiomyopathy. *J Am Coll Cardiol*. 2000;35:19–28.
109. Kato S, Saito N, Kirigaya H, Gyotoku D, Iinuma N, Kusakawa Y, Iguchi K, Nakachi T, Fukui K, Futaki M, Iwasawa T, Kimura K, Umemura S. Impairment of coronary flow reserve evaluated by phase contrast cine-magnetic resonance imaging in patients with heart failure with preserved ejection fraction. *J Am Heart Assoc*. 2016;5:pii: e002649. doi: 10.1161/JAHA.115.002649.
110. Mohammed SF, Hussain S, Mirzoyev SA, Edwards WD, Maleszewski JJ, Redfield MM. Coronary microvascular rarefaction and myocardial fibrosis in heart failure with preserved ejection fraction. *Circulation*. 2015;131:550–559. doi: 10.1161/CIRCULATIONAHA.114.009625.
111. Paulus WJ, Tschöpe C. A novel paradigm for heart failure with preserved ejection fraction: comorbidities drive myocardial dysfunction and remodeling through coronary microvascular endothelial inflammation. *J Am Coll Cardiol*. 2013;62:263–271. doi: 10.1016/j.jacc.2013.02.092.
112. Srivaratharajah K, Coutinho T, deKemp R, Liu P, Haddad H, Stadnick E, Davies RA, Chih S, Dwivedi G, Guo A, Wells GA, Bernick J, Beanlands R, Mielniczuk LM. Reduced Myocardial Flow in Heart Failure Patients With Preserved Ejection Fraction. *Circ Heart Fail*. 2016;9:pii: e002562. doi: 10.1161/CIRCHEARTFAILURE.115.002562.
113. Rajappan K, Rimoldi OE, Camici PG, Bellenger NG, Pennell DJ, Sheridan DJ. Functional changes in coronary microcirculation after valve replacement in patients with aortic stenosis. *Circulation*. 2003;107:3170–3175. doi: 10.1161/01.CIR.0000074211.28917.31.
114. Rajappan K, Rimoldi OE, Dutka DP, Ariff B, Pennell DJ, Sheridan DJ, Camici PG. Mechanisms of coronary microcirculatory dysfunction in patients with aortic stenosis and angiographically normal coronary arteries. *Circulation*. 2002;105:470–476.
115. Wiegerinck EM, van de Hoef TP, Rolandi MC, Yong Z, van Kesteren F, Koch KT, Vis MM, de Mol BA, Piek JJ, Baan J Jr. Impact of aortic valve stenosis on coronary hemodynamics and the instantaneous effect of transcatheter aortic valve implantation. *Circ Cardiovasc Interv*. 2015;8:e002443. doi: 10.1161/CIRCINTERVENTIONS.114.002443.
116. Kofoed KF, Czernin J, Johnson J, Kobashigawa J, Phelps ME, Laks H, Schelbert HR. Effects of cardiac allograft vasculopathy on myocardial blood flow, vasodilatory capacity, and coronary vasomotion. *Circulation*. 1997;95:600–606.
117. Mc Ardle BA, Davies RA, Chen L, Small GR, Ruddy TD, Dwivedi G, Yam Y, Haddad H, Mielniczuk LM, Stadnick E, Hessian R, Guo A, Beanlands RS, deKemp RA, Chow BJ. Prognostic value of rubidium-82 positron emission tomography in patients after heart transplant. *Circ Cardiovasc Imaging*. 2014;7:930–937. doi: 10.1161/CIRCIMAGING.114.002184.
118. Dorbala S, Vangala D, Bruyere J Jr, Quarta C, Kruger J, Padera R, Foster C, Hanley M, Di Carli MF, Falk R. Coronary microvascular dysfunction is related to abnormalities in myocardial structure and function in cardiac amyloidosis. *JACC Heart Fail*. 2014;2:358–367. doi: 10.1016/j.jchf.2014.03.009.
119. Fukushima K, Javadi MS, Higuchi T, Bravo PE, Chien D, Lautamäki R, Merrill J, Nekolla SG, Bengel FM. Impaired global myocardial flow dynamics despite normal left ventricular function and regional perfusion in chronic kidney disease: a quantitative analysis of clinical 82Rb PET/CT studies. *J Nucl Med*. 2012;53:887–893. doi: 10.2967/jnumed.111.099325.
120. Shah NR, Charytan DM, Murthy VL, Skali Lami H, Veeranna V, Cheezum MK, Taqueti VR, Kato T, Foster CR, Hainer J, Gaber M, Klein J, Dorbala S, Blankstein R, Di Carli MF. Prognostic value of

coronary flow reserve in patients with dialysis-dependent ESRD. *J Am Soc Nephrol*. 2016;27:1823–1829. doi: 10.1681/ASN.2015030301.

121. Ikonomidis I, Lekakis JP, Nikolaou M, Paraskevaidis I, Andreadou I, Kaplanoglou T, Katsimbri P, Skarantavos G, Soucacos PN, Kremastinos DT. Inhibition of interleukin-1 by anakinra improves vascular and left ventricular function in patients with rheumatoid arthritis. *Circulation*. 2008;117:2662–2669. doi: 10.1161/CIRCULATIONAHA.107.731877.
122. Recio-Mayoral A, Mason JC, Kaski JC, Rubens MB, Harari OA, Camici PG. Chronic inflammation and coronary microvascular dysfunction in patients without risk factors for coronary artery disease. *Eur Heart J*. 2009;30:1837–1843. doi: 10.1093/eurheartj/ehp205.
123. Nitenberg A, Foult JM, Kahan A, Perennec J, Devaux JY, Menkes CJ, Amor B. Reduced coronary flow and resistance reserve in primary scleroderma myocardial disease. *Am Heart J*. 1986;112:309–315.
124. Neglia D, Michelassi C, Trivieri MG, Sambuceti G, Giorgetti A, Pratali L, Gallopin M, Salvadori P, Sorace O, Carpeggiani C, Poddighe R, L'Abbate A and Parodi O. Prognostic role of myocardial blood flow impairment in idiopathic left ventricular dysfunction. *Circulation*. 2002;105:186–93.